The timing and cause of glacial advances in the southern mid-latitudes during the last glacial cycle based on a synthesis of exposure ages from Patagonia and New Zealand

Christopher M. Darvill*[1,†], Michael J. Bentley[1], Chris R. Stokes[1] & James Shulmeister[2]

*E-mail: christopher.darvill@unbc.ca

[1]Department of Geography, Durham University, South Road, Durham, DH1 3LE, UK.

[2]School of Geography Planning and Environmental Management, University of Queensland, Brisbane, QLD 4072, Australia.

†Present address: Geography Program and Natural Resources and Environmental Studies Institute, University of Northern British Columbia, 3333 University Way, Prince George, BC, V2N 4Z9, Canada.

Abstract

Glacier advances in the southern mid-latitudes during the last glacial cycle (*ca*. 110-10 ka) were controlled by changes in temperature and precipitation linked to several important ocean-climate systems. As such, the timing of glacial advance and retreat can yield important insights into the mechanisms of Southern Hemisphere climate change. This is particularly important given that several recent studies have demonstrated significant glacial advances prior to the global Last Glacial Maximum (gLGM) in Patagonia and New Zealand, the cause of which are uncertain. The recent increase in chronological studies in these regions offers the opportunity to compare regional trends in glacial activity. Here, we compile the first consistent ^{10}Be exposure-dating chronologies for Patagonia and New Zealand to highlight the broad pattern of mid-latitude glacial activity over the last glacial cycle. Our results show that advances or still stands culminated at 26-27 ka, 18-19 ka, 13-14 ka in both Patagonia and New Zealand and were broadly synchronous, but with an offset between regions of up to 900 years that cannot be explained by age calculation or physically plausible erosion differences. Furthermore, there is evidence in both regions for glacial advances culminating from at least 45 ka, during the latter half of Marine Isotope Stage (MIS) 3. Glacial activity prior to the gLGM differ from the large Northern Hemisphere ice sheets, likely due to favourable Southern Hemisphere conditions during late MIS 3: summer insolation reached a minimum, seasonality was reduced, winter duration was increasing, and sea ice had expanded significantly, inducing stratification of the ocean and triggering northward migration of oceanic fronts and the Southern Westerly Winds. Glacial advances in Patagonia and New

Zealand during the gLGM were probably primed by underlying orbital parameters. However, the precise timing is likely to have been intrinsically linked to migration of the coupled ocean-atmosphere system, which may account for the small offset between Patagonia and New Zealand due to differences in oceanic frontal migration. During deglaciation, advances or still stands occurred in both regions during the southern Antarctic Cold Reversal (*ca*. 14.5-12.9 ka) rather than the northern Younger Dryas (*ca*. 12.9-11.7 ka). Our findings suggest that major rearrangements of the Southern Hemisphere climate system occurred at various times during the last glacial cycle, with associated impacts on the position and intensity of the Southern Westerly Winds and oceanic fronts, as well as wind-driven upwelling and degassing of the deep Southern Ocean. Thus, reconstructing the timing of glacial advance/retreat using our compilation is a powerful way to understand the mechanisms of past interhemispheric climate change.

1 Introduction

Patagonia, in southern South America, and South Island, New Zealand, hosted the two largest non-Antarctic ice masses in the Southern Hemisphere during Quaternary glaciations (Coronato & Rabassa, 2011; Barrell, 2011; Figure 1). The former Patagonian Ice Sheet extended from the Andean range to cover significant parts of Chile and Argentina between ~36 and ~56°S (Figure 2), and the New Zealand icefield occupied much of the Southern Alps between ~40 and ~46°S (Figure 3). Together, glaciers extending from these two ice masses covered a broad latitudinal range in the southern mid-latitudes and were influenced by important global ocean-climate systems. These include the oceanic Sub Tropical, Sub Antarctic and Polar Fronts, the Antarctic Circumpolar Current and Agulhaus Current leakage, and the position and/or strength of the Southern Westerly Wind system. Moreover, a number of modes of variability such as the Southern Annular Mode and embedded phenomena in the three Walker Circulations (e.g. the Indian Ocean Dipole and El Niño Southern Oscillation) may have influenced glacier behaviour. As a result, glacial records from Patagonia and New Zealand have the potential to improve our understanding of global climate teleconnections and have been widely used to reconstruct past climatic change.

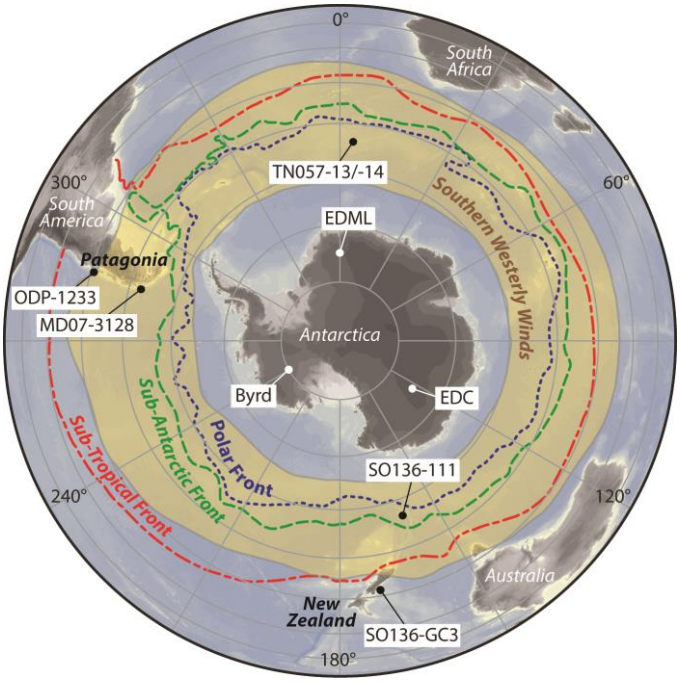

Figure 1. Map of the Southern Hemisphere showing the modern positions of the Sub-Tropical Front (red), Sub-Antarctic Front (green) and Polar Front (blue), as well as the core region of the Southern Westerly Winds (yellow-brown) and the locations of ice and marine core records referred to in the text. Note the latitudinal difference of the oceanic frontal systems around Patagonia compared to New Zealand.

Recent work (Glasser et al., 2011; Putnam et al., 2013b; Kelley et al., 2014; Rother et al., 2014; Doughty et al., 2015; Schaefer et al., 2015; Darvill et al., 2015) has identified that some glaciers in Patagonia and New Zealand advanced to greater extents prior to the global Last Glacial Maximum (gLGM; *ca*. 26.5-19 ka; Clark et al., 2009) and Marine Isotope Stage (MIS) 2. This is not necessarily surprising: Hughes et al., (2013) suggested that many ice sheets around the world did not achieve maximum extent at the same time during the last glacial cycle (*ca*. 110-10 ka). However, it does indicate that our understanding of southern mid-latitude glacial advances might be incomplete, with implications for our understanding of southern climate systems more generally. Specifically, the new glacial chronologies raise two important issues. First, it is unclear whether pre-gLGM glacial advances were representative of the Patagonian and New Zealand ice masses more broadly and, if so, whether they were synchronous across the southern mid-latitudes. Secondly, the forcing factors behind southern mid-latitude glaciation during the last glacial cycle are ambiguous, as is the relationship to climatic drivers in the Northern Hemisphere. For example, insolation does not appear to directly control Southern Hemisphere climate change (Huybers & Denton, 2008; Doughty et al., 2015), whereas the movement of the southern westerly winds and oceanic frontal systems have been invoked as drivers of climate and glacial advances by controlling precipitation and sea surface temperatures (Lamy et al., 2004, 2007; Barrows

et al., 2007a; Denton et al., 2010). The roles of sea ice and ocean stratification, whilst likely important, also remain unclear (Allen et al., 2011; Denton et al., 2010; Putnam et al., 2013b). Moreover, the interplay between Southern and Northern Hemisphere climate systems is particularly contentious (Sugden et al., 2005), with some suggesting that global climate is driven by changes in the north (e.g. Denton et al., 2010) and others advocating initial triggers in the south (e.g. Wolff et al., 2009).

Tackling these problems requires a synthesis of the evidence for the timing of glacial activity in Patagonia and New Zealand. Given the high volume of new chronological data that has been published in recent years, this paper compiles glacial chronologies for both regions during the last glacial cycle to examine, for the first time, if similar trends are evident and whether these are replicated over large geographic areas. We then compare the timing of culminations of glacial advances with terrestrial, marine and ice core proxy records and test hypotheses regarding how southern climatic systems operated through time. Whilst other ice caps and glaciers existed in Chile, Australia, Tasmania, North Island (New Zealand) and elsewhere in the sub-Antarctic during the last glacial cycle, we limit our focus to Patagonia and South Island. This is because they hosted the largest ice masses and produced similarly-detailed and well-preserved glacial records that have been studied in the greatest detail. We primarily focus on ^{10}Be cosmogenic nuclide dating because it offers direct age estimates for glacial moraine records and has been used extensively in both regions.

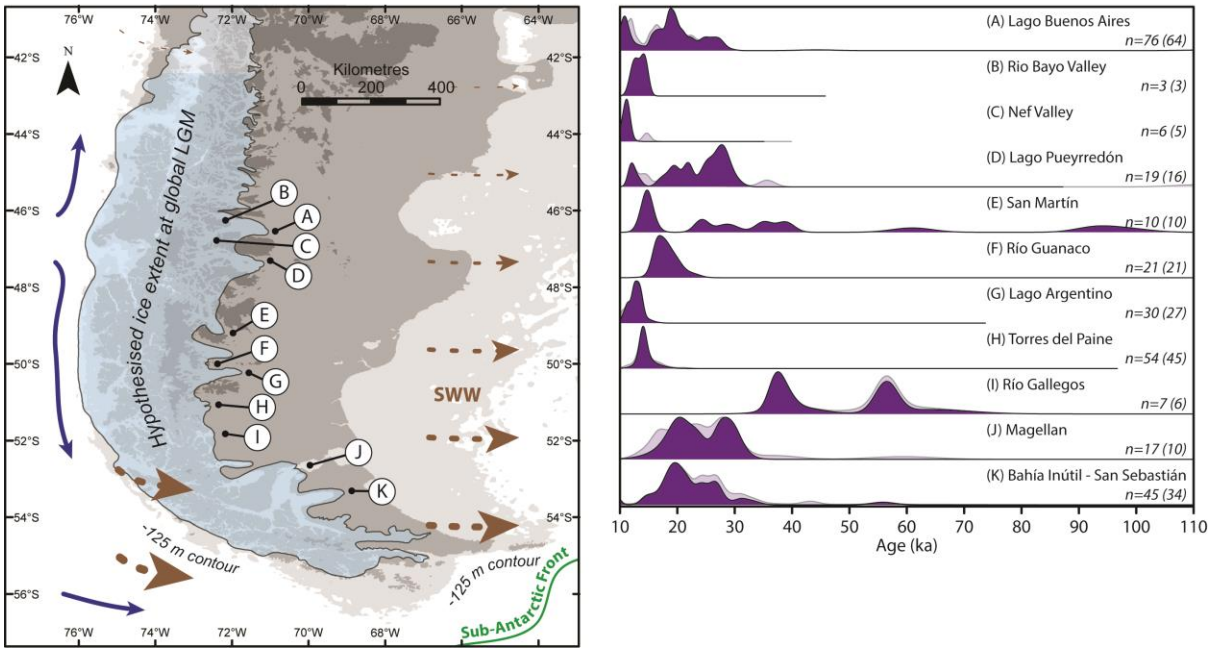

Figure 2. (Left) Map of Patagonia, showing the hypothesised extent of the gLGM ice sheet from Coronato & Rabassa (2011) and -125 m bathymetric contour to give an impression of the likely drop in sea-level at the time. Glacial valleys or systems used in this study are labelled (A-K; corresponding to names on the right) as well as major oceanic circulations (blue arrows), Southern Westerly Wind direction (brown dashed arrows), and the Sub-Antarctic Front (green line). (Right) Probability density functions for each glacial system consisting of all exposure ages (lighter shading) and with author-identified outliers removed (darker shading), normalised in both cases. The numbers of exposure ages relating to each system are shown without and with (in brackets) outliers removed.

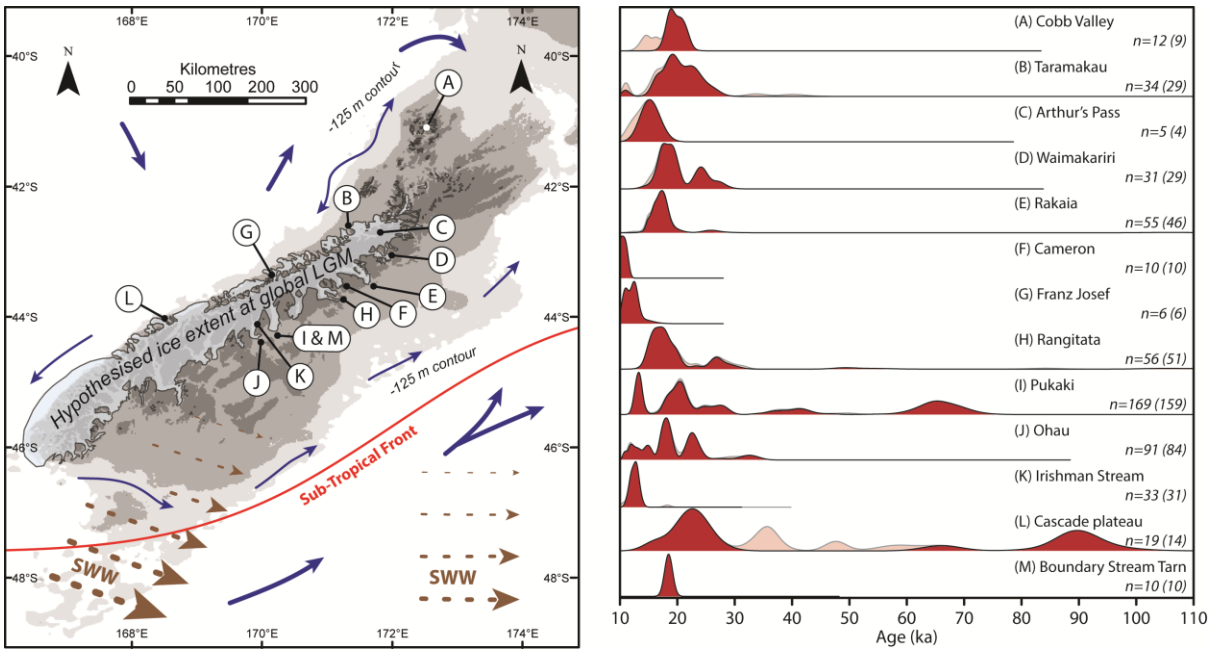

Figure 3. (Left) Map of South Island, New Zealand, showing the hypothesised extent of the gLGM ice sheet from Barrell (2011) and -125 m bathymetric contour to give an impression of the likely drop in sea-level at the time. Glacial valleys or systems used in this study are labelled (A-K; corresponding to names on the right) as well as major oceanic circulations (blue arrows), Southern Westerly Wind direction (brown dashed arrows), and the Sub-Tropical Front (red line). (Right) Probability density functions for each glacial system consisting of all exposure ages (lighter shading) and with author-identified outliers removed (darker shading), normalised in both cases. The numbers of exposure ages relating to each system are shown without and with (in brackets) outliers removed.

2 Methods

Our compilation consists of ^{10}Be cosmogenic nuclide exposure data from studies across Patagonia and New Zealand (Figures 2 and 3; Table 1). We collated published ^{10}Be exposure ages for moraine boulders and outwash cobbles, which record the timing of the onset of glacial retreat following an advance (Figure 4). Only two studies have used outwash cobbles in this manner, and in both cases they are essentially equivalent to exposure ages from boulders (Hein et al., 2009; Darvill et al., 2015). We excluded bedrock and moraine cobble samples due to potential issues with re-setting and because they do not necessarily represent glacial activity in the same way. For consistency, we recalculated all exposure ages, applying the Putnam et al. (2010) New Zealand ^{10}Be production rate for exposure ages in New Zealand and Patagonia, as well as the Kaplan et al. (2011) Patagonian ^{10}Be production rate for exposure ages in Patagonia. We also calculated ages using five scaling schemes and a range of erosion rates (1 mm ka^{-1} intervals between 0 and 10 mm ka^{-1}) to evaluate the effects of these parameters on age distributions (Figure 5). All other parameters, including standards, were taken from the original literature or subsequent updates (e.g. Kaplan et al., 2011), and we used a standard density of 2.7 g cm^{-3} where none was given in the original studies. To aid the identification of cumulative peaks in exposure time we employed cumulative Probability Density Functions (PDFs; Barrows et al., 2002) using 100-year bins, and excluded any exposure ages that, within errors, fall outside the last glacial cycle between 110 and 10 ka.

3 Results

3.1 ^{10}Be chronology and outliers

Glacial systems have yielded cosmogenic nuclide exposure ages throughout the last glacial cycle and, since *ca*. 45 ka, show a similar pattern in Patagonia and New Zealand (Figure 4; Table 2). In contrast exposure ages prior to 45 ka are more scattered or are not reproduced across different glacial systems. There are also significant gaps in the record, with few or no exposure ages between 79 and 110 ka (MIS 5). A key goal of this study is to assess a large compilation dataset to see if there are regional trends that have previously been missed in individual studies. Therefore, it is important to ensure that author-identified outliers were not removed erroneously. We calculated all of the ages twice, once with all data included ($n_{Patagonia}$ = 289; $n_{New\ Zealand}$ = 531) and the second time with all author-identified outliers removed ($n_{Patagonia}$ = 241; $n_{New\ Zealand}$ = 482; Figure 5; Table 1). We only removed outliers that were clearly identified in the original studies and if there was any ambiguity, we retained the

data. Removing author-identified outliers made negligible difference to the timing of the compiled PDF peaks, and so the reduced compilation was used for all other analysis in this paper.

3.2 Examining peaks in ^{10}Be timing

Peaks in the PDF plots for all exposure ages in Patagonia and New Zealand help to illustrate times when a larger number of glaciers started to retreat. This technique is useful for identifying patterns in a large number of exposure ages, but should be used with caution, as it does not convey the spatial distribution (e.g. down-ice extent) of exposure ages and can be influenced by uncertainty in factors such as erosion rate and inheritance during age calculation (factors which we explore in the following sections). Different glaciers within the compilation likely advanced and retreated at different times, and the PDF technique removes this subtle variability. In a discussion about the possible forcing factors responsible for regional glacial activity, we are interested in the commonality between the timing of glacial retreat from a robust chronological dataset, so this approach is useful. It is important to note that the fact that our compilation produces clear PDF peaks at all implies that there is regional commonality in the timing of glacial activity during the last glacial cycle.

The timing of PDF peaks in Patagonia and New Zealand are shown in Table 2. Peaks at 56.4 ka (Patagonia), 65.3 ka and 89.7 ka (New Zealand) are intriguing, especially at 65.3 ka, which is largely attributable to a focused study of the former Pukaki Glacier by Schaefer et al. (2015). However, because the replication of exposure ages between glaciers is much weaker prior to 45 ka, we focus on peaks after this time. Table 2 shows broad commonality of peaks after 45 ka, but there appears to be a variable offset between Patagonia and New Zealand in the timing of the three dominant PDF peaks. These peaks are at 26-27 ka (with an offset of 300 years between the Patagonia and New Zealand peaks), 18-19 ka (with an offset of 700 years) and 13-14 ka (with an offset of 900 years). The PDF peaks occur in Patagonia before New Zealand and the offset decreases back in time (Table 2). Before exploring whether there is a geographical or climatological reason for this effect, it is first necessary to examine whether factors inherent in the age calculation process can account for the offset. Specifically, we assess sensitivity to the production rate or scaling scheme used; the erosion rate applied; possible inheritance issues; or analytical uncertainty. This exercise is also useful for assessing how the overall spread of ages changes when these parameters are varied.

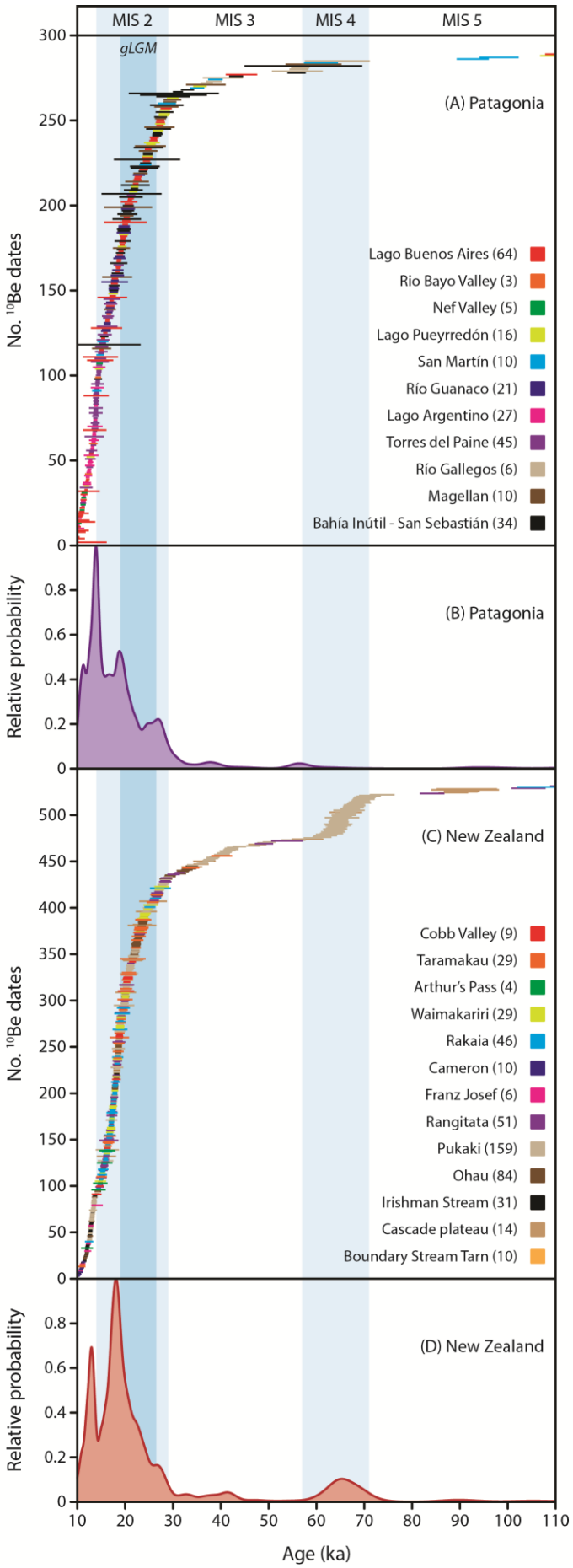

Figure 4. The compilation of ^{10}Be exposure ages from Patagonia and New Zealand used in this study (see Table 1), shown against the Marine Isotope Stages from Lisiecki & Raymo (2005) and the gLGM from Clark et al. (2009). (A and C) For Patagonia and New Zealand, respectively: all ^{10}Be exposure ages within 110-10 ka, including author-identified outliers, as mean ages with standard errors recalculated using the Putnam et al. (2010b) production rate, with no erosion rate applied. The exposure ages are colour-coded according to the glacial system from which they are derived, and associated references can be found in Table 1. (B and D) For Patagonia and New Zealand, respectively: normalised cumulative relative probability density function curves, calculated from all of the exposure ages shown in (A and C).

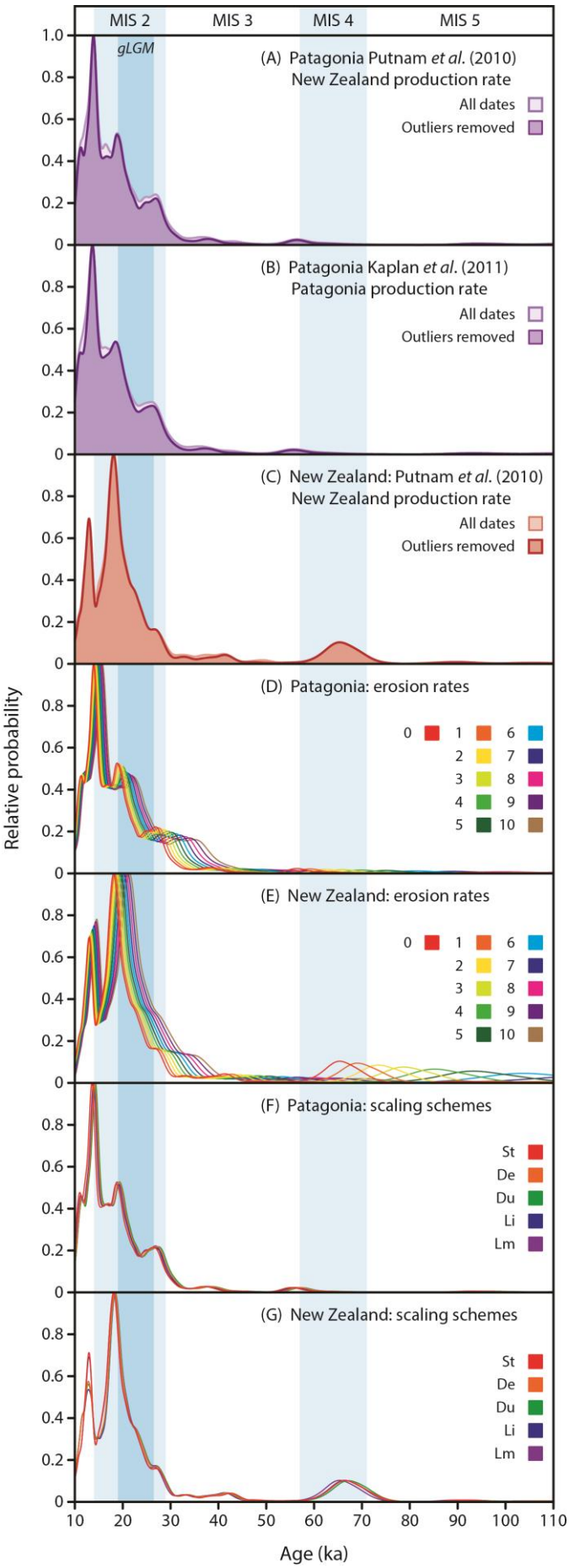

Figure 5. Examining the effects of calculation parameters on the overall spread of ages in our compilation. (A, B and C) Normalised probability density functions from Figure 4 without and with author-identified outliers removed. There is little resulting difference in the timing of peaks. (B) The effect of calculating all exposure ages from Patagonia with the Patagonian production rate of Kaplan et al. (2011). (D and E) The effect on the resulting normalised probability density functions of incrementally increasing the erosion rate by 1 mm ka-1 during the calculation of all ages in Patagonia and New Zealand. The timing of peaks can be found in Table 2. (F and G) The effect of altering the scaling scheme used. The scaling schemes are: the time-independent Lal (1991) and Stone (2000; St); Desilets et al. (2006; De); Dunai (2001; Du); Lifton et al. (2005; Li); and time-dependent Lal (1991) and Stone (2000; Lm). In (D, E, F and G), all author-identified outliers have been removed, the New Zealand production rate is used and, where relevant, no erosion rate is applied.

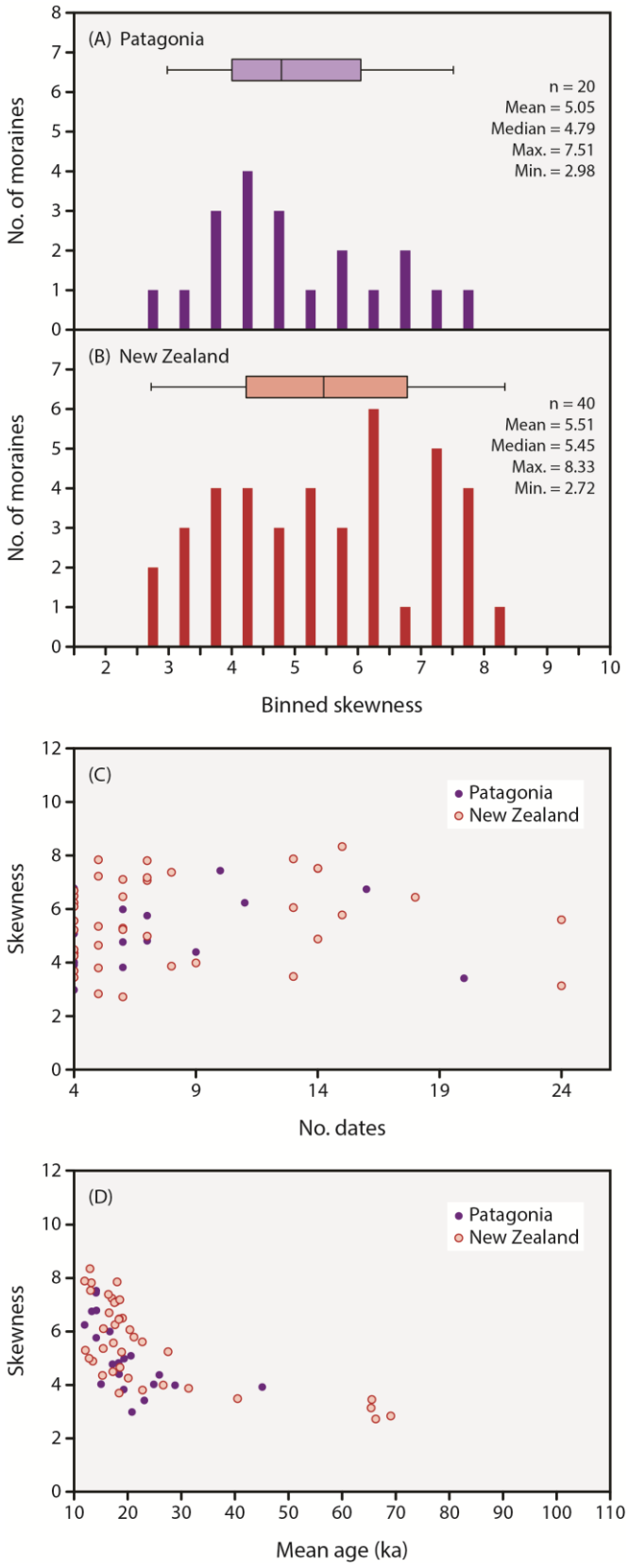

Figure 6. (A and B) Binned results from an analysis of skewness of probability density functions from individual moraine sets in Patagonia and New Zealand as a crude proxy for differential inheritance signatures. The data suggest that inheritance cannot fully explain the consistent offset between Patagonia and New Zealand. (C and D) Skewness results against the number of exposure ages per moraine and age, respectively, demonstrating that these variables do not influence skewness (i.e. inheritance) in Patagonia more or less than New Zealand. (D) Younger moraines in both regions show greater skewness, indicating greater inheritance. See main text for discussion.

3.2.1 Production rate and scaling scheme

An offset in the timing of PDF peaks in Patagonia and New Zealand could be an artefact of recalculating all ages using the New Zealand production rate, even though this overlaps with the Patagonian production rate at 1σ. Figure 5 and Table 2 show all exposure ages recalculated using the Putnam et al. (2010) Macaulay River, New Zealand, ^{10}Be production rate of 3.74 ± 0.08 atoms g^{-1} a^{-1}, and also the Patagonian exposure ages recalculated using the Kaplan et al. (2011) Lago Argentino, Patagonia, ^{10}Be production rate of 3.81 ± 0.13 atoms g^{-1} a^{-1}. The production rate alone can only explain the offset in PDF peaks at 26-27 ka, although these peaks are very similar in age, regardless of the production rate used. When recalculated using the Patagonian production rate, the 16.7 ka peak can no longer be resolved and the 26.9 ka and 18.8 ka peaks become broader.

We also calculated ages using different scaling schemes (Figure 5; using just the New Zealand production rate). It is illogical to use different scaling schemes for the Patagonian and New Zealand datasets, so the important part of this analysis is to see whether the choice of scaling scheme can account for a discrepancy in the timing of PDF peaks. While the choice of scaling scheme can alter the timing (by as much as 1.7 ka for the 37.8 ka peak in Patagonia) it cannot explain any differences between Patagonia and New Zealand.

3.2.2 Surface erosion rate

Differential surface erosion rates in Patagonia or New Zealand could have affected the timing of PDF peaks because increased erosion offsets the build-up of ^{10}Be nuclides, artificially yielding younger ages. To test the effects of the selected erosion rate, we recalculated all ages using increasing rates between 0 mm ka^{-1} and 10 mm ka^{-1} (Figure 5 and Table 2). The difference in the erosion rate required for the peaks in New Zealand to match Patagonia varied non-uniformly from 6 mm ka^{-1} to 0 mm ka^{-1}, and decreased back in time. At high erosion rates (> 6 mm ka^{-1}), some of the peaks flattened-out because there were insufficient high-precision exposure ages. Overall, high (though not necessarily unreasonable, see Kaplan et al. (2007)) erosion rates are required for the 13-14 ka peaks to have been synchronous in Patagonia and New Zealand. Lower erosion rates are required for the 18-19 ka and 26-27 ka peaks to have been synchronous.

3.2.3 Inheritance

Consistent inheritance in boulder populations in Patagonia could potentially have resulted in an offset in PDF peaks compared to New Zealand. To test this, we constructed PDF plots for moraine age populations. The shape of the PDF was heavily influenced by the number of boulder samples from each moraine if the plot was constructed from less than four samples, so we excluded all age populations containing three exposure ages or fewer, and removed any age populations that were not completely resolved between 10 and 110 ka. We then used a skewness test to examine if age populations showed greater inheritance in either region – a simplified approach to the modelling of Applegate et al. (2010), where we took positive skew in a moraine PDF distribution to indicate outliers due to increased inheritance. A consistent positive skew in one region compared to another might indicate that greater levels of inheritance influenced the timing of PDF peaks. Author-identified outliers had already been removed, so any inheritance-skew was in addition to the outliers that had already been removed (Figure 6). New Zealand contained moraine age populations that were more skewed (mean = 5.51; max. = 8.33) than Patagonia (mean = 5.05; max = 7.51). This relationship was not influenced by the number of exposure ages from each moraine and there is no difference in the relationship between moraine age and skew over time between the two regions. Consequently, inheritance cannot explain the offset between PDF peaks, as greater inheritance in New Zealand compared to Patagonia would only serve to have increased the age difference. Interestingly, it appears that the range of skew values is greater for younger moraines in both Patagonia and New Zealand (Figure 6D). This might imply greater inheritance in younger moraines, possibly linked to re-working of older moraine boulders, although the trend may be influenced by sampling techniques.

3.2.4 Analytical uncertainty

Assessing whether differences between two cosmogenic nuclide datasets are the result of differences in analytical uncertainty is particularly challenging. This is because it is rare for the same samples to be analysed by different laboratories; indeed, there are no such examples in our compilation. We examined the Rakaia Valley system in New Zealand – the only location in our study in which the same glacial sequence (but not the same samples) has been analysed by two different preparatory/AMS laboratories (see Shulmeister et al., 2010 and Putnam et al., 2013a). Comparing the exposure ages produced by the two studies appears to suggest that analytical uncertainty could account for as much as a 1.3 ka difference in the timing of exposure age PDF peaks (supplementary figure). However, in reality, this comparison means little because: (1) the analysis was conducted on different

samples; (2) the populations consist of different numbers of samples; and (3) there was uncertainty in comparing the geomorphic context of the two studies (Putnam et al., 2013a). Ultimately, we cannot discount analytical uncertainty as a potentially important factor in affecting the timing of PDF peaks, but we note that many laboratory groups have produced exposure ages from both Patagonia and New Zealand. Consequently, we have no reason to suspect that analytical uncertainty has caused a consistent offset between the two regions.

3.2.5 Summary: Offset of peaks in timing

Production rate, scaling scheme, erosion rate and inheritance all have an effect on the calculation of ages from ^{10}Be data, but none of these factors can provide a satisfactory explanation for the offset between Patagonia and New Zealand at 26-27 ka, 18-19 ka and 13-14 ka. This is because the offset does not decrease or increase uniformly back in time. Changing the scaling scheme does not reduce the offset, and using the Patagonian production rate neither reduces the offset sufficiently, nor accounts for a variable offset over time. Increasing the erosion rate in New Zealand can reduce the offset, but does not explain why the difference decreases back in time, and it is unlikely that inheritance is responsible for the difference. A combination of these factors may explain the offset observed in the timing of PDF peaks in Patagonia and New Zealand, but this starts to invoke cyclical arguments, some of which are themselves climate-related (e.g. variable erosion rates over time). A simpler explanation, which we prefer, is that the offset is real and PDF peaks in Patagonia occurred earlier than in New Zealand at 26-27 ka, 18-19 ka and 13-14 ka. We now discuss the timing of these peaks and their possible causes.

4 Discussion

4.1 The timing of glacial activity

4.1.1 Evidence from the compilation of exposure ages

We interpret the peaks in the PDF distributions at *ca*. 41.3 ka, 37.8 ka, 32.7 ka, 26-27 ka, 18-19 ka and 13-14 ka to reflect the deposition of moraine boulders and cobbles during the culminations of glacial advances or, at the very least, still stands during retreat. The resolution of these events is determined in part by sampling strategies that have targeted glacial limits and the corresponding dating errors – hence the gLGM and late glacial peaks are the best-resolved in both regions. This does not mean that the pre-gLGM limits were necessarily less distinct, and our method says little about the extent of limits other than that

they were preserved. It is also important to note that Putnam et al. (2010a) found closely-spaced moraines in one New Zealand valley that yielded exposure ages differing by *ca*. 1 ka, but this signal is not well represented in the compilation. Nonetheless, our ^{10}Be compilation from Patagonia and New Zealand reveals a broad similarity in the timing of glacial activity in both regions, especially during MIS 3 and MIS 2. This suggests that the same forcing factors may have controlled the timing of glacial activity in both regions over the last glacial cycle and strongly suggests that glaciers advanced by at least 45 ka, or mid-MIS 3, well before the gLGM. Although this study focuses on chronology, it is worth highlighting that several studies found the limits relating to these advances to be as extensive, if not significantly more extensive, than those deposited during the gLGM (Glasser et al., 2011; Putnam et al., 2013b; Kelley et al., 2014; Rother et al., 2014; Doughty et al., 2015; Darvill et al., 2015; Schaefer et al., 2015).

A large dataset of minimum and maximum radiocarbon dates for the Chilean Lake District was constructed by Denton et al. (1999) to constrain the timing of glacial activity, recently extended by Moreno et al. (2015). The radiocarbon data demonstrate glacial advances at *ca*. 33.6 ka, 30.8 ka, 26.9 ka, 26.0 ka and 17.7-18.1 ka (Moreno et al., 2015), which is consistent with our compiled ^{10}Be peaks at 26.9 ka and 18 ka and pre-30 ka during the last glacial cycle across Patagonia. The replication of ^{10}Be exposure ages over multiple glaciers in Patagonia and New Zealand, supported by radiocarbon dates, gives us confidence in discussing peaks in the timing of deposition as regional culminations of glacial advances. We now compare these events with other proxies for glacial and climatic change in order to assess possible forcing mechanisms within the terrestrial-ocean-atmosphere system during the last glacial cycle (Figures 7 and 8).

4.1.2 Late MIS 5 (ca. 110-71 ka)

Little evidence exists for glacial activity during MIS 5, with only occasional exposure ages from individual glaciers around 90 ka (Sutherland et al., 2007; Glasser et al., 2011) that change significantly with slight alterations in erosion rate (Figure 5). Low Antarctic dust concentrations (Fischer et al., 2007) support the absence of glacial activity, particularly in Patagonia (Sugden et al., 2009; Kaiser & Lamy, 2010; McGee et al., 2010; Figure 8K). Antarctic temperatures were warmer, but with millennial-scale variability (EPICA, 2006), including a cooling between *ca*. 92 ka and 87 ka (Figure 8B, C and D) that is also recorded in local Sea Surface Temperatures (SSTs; Barrows et al., 2007a) and preceded a decline in New Zealand forest pollen after 82 ka (Ryan et al., 2012; Vandergoes et al., 2013). However, overall, MIS 5 was not likely to have promoted ice expansion in either region,

which is in contrast to the Northern Hemisphere where both the Northern American Ice Sheet complex and the Fennoscandian Ice Sheet are thought to have grown rapidly during MIS 5d (Clark et al., 1993; Kleman et al., 1997; Stokes et al., 2012).

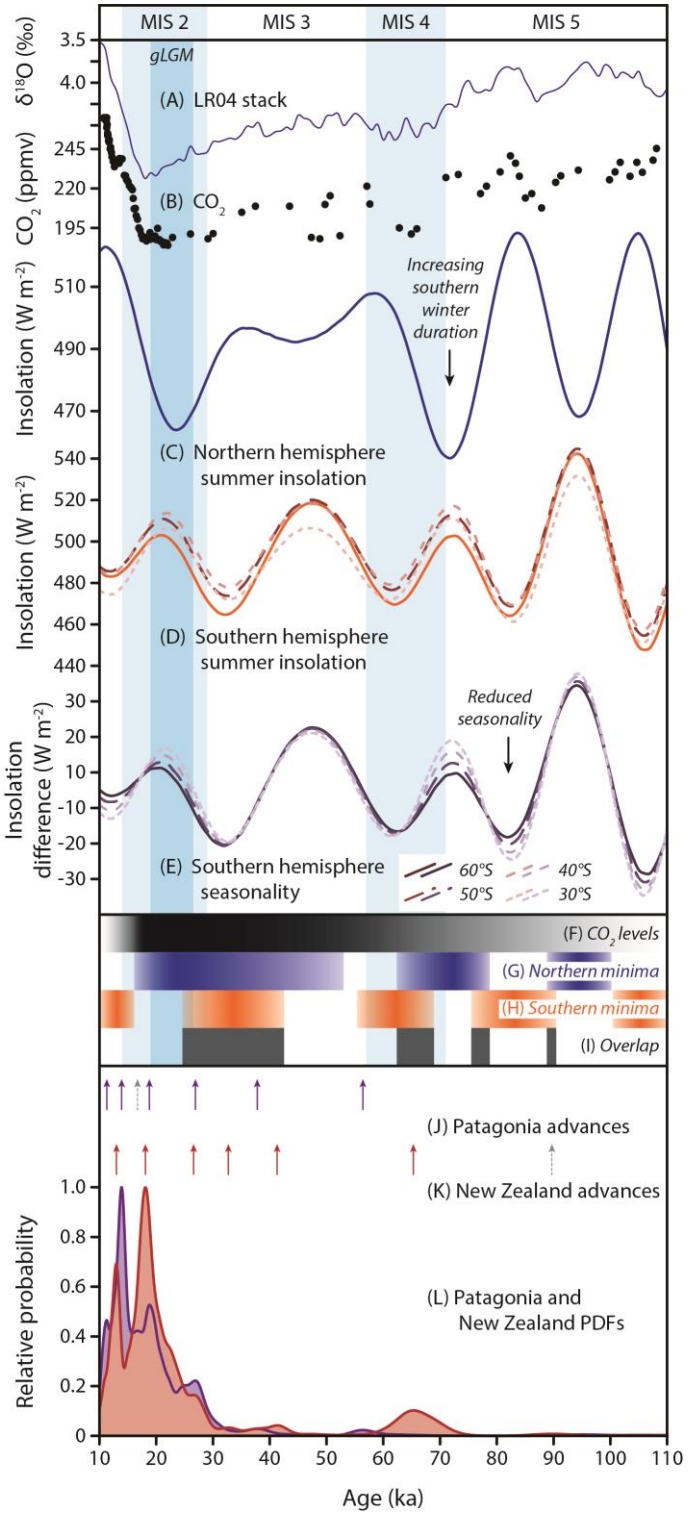

Figure 7. Orbital insolation parameters relevant to this study, from Berger & Loutre (1991). (A) LR04 benthic foraminiferal $\delta^{18}O$ stack (Lisiecki & Raymo, 2005), which shows a combined signature of global temperature and ice volume, (B) CO_2 record from EPICA Dome C (Lüthi et al., 2008), and (C) Northern Hemisphere summer (June) insolation intensity at 60°N. These three proxies show that global temperatures and Northern Hemisphere ice sheets followed Northern Hemisphere insolation during the last glacial cycle. (C) also shows Southern Hemisphere winter duration, given that decreasing northern summer insolation co-varies with increasing southern winter length (Huybers & Denton, 2008). (D) Southern Hemisphere summer (December) insolation intensity and (E) Southern Hemisphere seasonality at 60°S, 50°S, 40°S and 30°S. Seasonality values are calculated for each latitude by subtracting the June (winter) insolation from the December (summer) insolation at a given time, such that decreasing seasonality indicates cooler summers and warmer winters. These values are then normalised against the mean seasonality at each latitude for 110-10 ka. (F, G, H and I) Illustrations of decreasing CO_2 levels (F); Northern Hemisphere summer insolation intensity minima (G); Southern Hemisphere summer insolation intensity minima (H); and the broad overlap between the insolation minima in the Northern and Southern Hemispheres (I). The insolation intensity thresholds for these illustrations are entirely arbitrary: below 500 W m^{-2} for the Northern Hemisphere and below 490 W m^{-2} for the Southern Hemisphere (60˚S, except for the prolonged decreases at 93-85 ka and 47-34 ka, where threshold is raised). (J and K) The timing of peaks in our compilation for Patagonia and New Zealand, respectively, from Table 2. (L) Our ^{10}Be compilation from Patagonia and New Zealand with outliers removed.

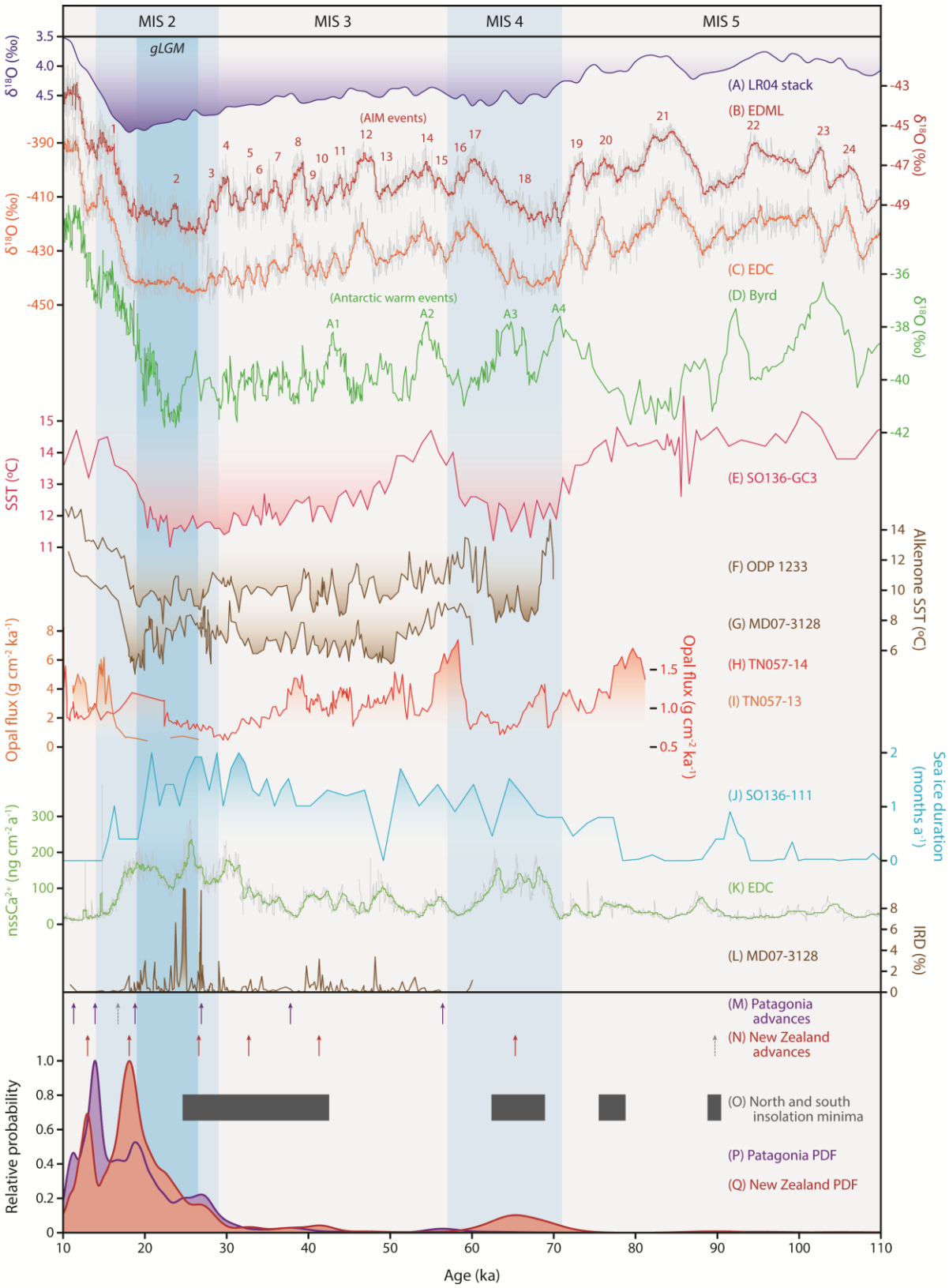
MIS 2
MIS 3
MIS 4
MIS 5
gLGM
(A) LR04 stack
(B) EDML
(AIM events)
(C) EDC
(D) Byrd
(Antarctic warm events)
(E) SO136-GC3
(F) ODP 1233
(G) MD07-3128
(H) TN057-14
(I) TN057-13
(J) SO136-111
(K) EDC
(L) MD07-3128
(M) Patagonia advances
(N) New Zealand advances
(O) North and south insolation minima
(P) Patagonia PDF
(Q) New Zealand PDF
δ18O (‰)
SST (°C)
Opal flux (g cm-2 ka-1)
nssCa2+ (ng cm-2 a-1)
Alkenone SST (°C)
Sea ice duration (months a-1)
IRD (%)
Relative probability
Age (ka)

Figure 8. A comparison of the timing of glacial advances in the southern mid-latitudes during 110-10 ka with a range of other palaeoclimatic proxies. (A) The LR04 benthic foraminiferal stack (Lisiecki & Raymo, 2005). (B) The East Dronning Maud Land (EDML) ice core $\delta^{18}O$ record (EPICA, 2006); (D) the EPICA Dome C (EDC) ice core δD record (EPICA, 2006); and (E) the Byrd ice core $\delta^{18}O$ record (Blunier & Brook, 2001) as proxies for Antarctic temperature changes from different parts of the ice sheet. The EDML and EDC records are shown on the AICC2012 common timescale (Veres et al., 2013), whereas the Byrd ice core is plotted on its own timescale. (E) Faunal-based Sea Surface Temperature (SST) record from core SO136-GC3 as a proxy for regional temperature changes west of New Zealand (Barrows et al., 2007a). (F and G) Alkenone-derived SST reconstructions for ODP-1233 off the western coast of northern Patagonia (Kaiser et al., 2005) and for MD07-3128 off the western coast of southern Patagonia (Caniupán et al., 2011), both plotted on the same scale. (H and I) Records of opal flux from cores TN057-13 and -14 in the South Atlantic, south of the Polar Front, as a proxy for wind-driven upwelling (Anderson et al., 2009). Note that the scales are different. (J) Diatom-based reconstruction of sea ice extent from south of the Sub-Antarctic Front (Crosta et al., 2004), measured as the number of months per year that sea ice covered site SO136-111. (K) Ca^{2+} flux as recorded in the EDC ice core as a proxy for dust deposition over Antarctica, sourced predominantly from Patagonia (Fischer et al., 2007). (L) A record of Ice-Rafted Debris (IRD) from core MD07-3128 (Caniupán et al., 2011). (M and N) Peaks in the timing of glacial advances from Table 2. (O) Overlap between Northern Hemisphere and Southern Hemisphere summer insolation intensity minima from Figure 7. (P and Q) Our ^{10}Be compilation from Patagonia and New Zealand with outliers removed.

4.1.3 MIS 4 (ca. 71-57 ka)

There is limited evidence for glacial activity during MIS 4 from our dataset. Scattered exposure ages suggest that some glaciers expanded during this time and the Pukaki Glacier in New Zealand shows evidence for an MIS 4 advance around 65 ka (Schaefer et al., 2015; Figure 4), which would be consistent with a similarly-timed maxima in the Northern Hemisphere during MIS 4 (Clark et al., 1993; Stokes et al., 2012). The exposure ages from this glacier correlate with significant increases in dust production in the East Dronning Maud Land (EDML) and EPICA Dome C (EDC) Antarctic ice core records (Fischer et al., 2007; Wolff et al., 2006; EPICA, 2004, 2006; Figure 8K), and a reduction in upwelling (Anderson et al., 2009; Figure 8H). Antarctic temperatures show a marked cooling equivalent to the gLGM in the EDML and EDC ice cores until around 63 ka (EPICA, 2004, 2006; Figure 8B and C). There was a similar drop in localised SST records around New Zealand (Barrows et al., 2007a); Figure 8E) that is also reflected in speleothem records indicating cooler conditions at 67-63 ka and wetter conditions at 71-61 ka (Williams et al., 2015). An even greater SST reduction occurred off the west coast of northern Patagonia, where temperatures reached their lowest levels of the last glacial cycle (Kaiser et al., 2005; Figure 8F). Southern Hemisphere summer insolation was decreasing (Berger & Loutre, 1991), and there was a period of longer duration winters prior to MIS 4 (Huybers & Denton, 2008) followed by a period of decreased seasonality (Figure 7). Therefore, the evidence suggests that MIS 4 was a major cool period in the southern mid-latitudes, and should have instigated significant glacial advances across Patagonia and New Zealand. The absence of exposure ages from multiple glaciers suggests that either glacial activity was not as extensive as later advances, or that MIS 4 moraines have not been sufficiently sampled.

4.1.4 Early MIS 3 (ca. 57-45 ka)

Only scattered exposure ages have been recorded during early MIS 3, with a small peak in Patagonia at 56.4 ka. In this interval, dust and IRD records show little change beyond occasional small peaks (Fischer et al., 2007; Caniupán et al., 2011; Figure 8K and L) and SSTs were equivalent to those during the Holocene (Barrows et al., 2007a). Antarctic temperatures warmed following MIS 4 (EPICA, 2006), and early MIS 3 showed a strong millennial-scale pattern of warming and cooling into and out of the A4-1 events (Blunier & Brook, 2001; Figure 8D). The absence of prolonged cooling or build-up of sea-ice (Crosta et al., 2004; Wolff et al., 2006) suggests that these were only transient events and so may have prevented any significant glacial advances. In New Zealand, speleothem records suggest a cooler period at 51-45 ka (Williams et al., 2015), and the Te Anau cave stratigraphy suggests a glacial advance at *ca*. 48 ka (Williams, 1996). However, the Aurora Cave speleothem indicates continuous growth between 55.3 ka and 42.8 ka, implying local ice-free conditions at this time (Williams, 1996; Williams et al., 2015). The implication is that while millennial-scale events may have caused some glacial activity that is not well recorded in our compilation (e.g. between 50 ka and 46 ka), overall climatic conditions were not well suited for glacial advances during early MIS 3.

4.1.5 Late MIS 3 (ca. 45-29 ka)

There is evidence for glacial advances culminating during late MIS 3, at 37.8 ka in Patagonia, and 41.3 ka and 32.7 ka in New Zealand. In the same period there are small peaks in IRD off Patagonia (Caniupán et al., 2011), and increasing dust levels in the EDML and EDC ice cores towards the end of the period (Fischer et al., 2007; Figure 8K and L). Regionally, the EDML, EDC and Byrd ice cores show a cooling trend during MIS 3 (EPICA, 2006, 2004; Blunier & Brook, 2001; Figure 8B, C and D), mirroring the NGRIP record (Rasmussen et al., 2006), although this is overprinted by millennial-scale variability, including the A1 event (Blunier & Brook, 2001; EPICA, 2006; Wolff et al., 2009, 2010). Likewise, numerous SST reconstructions suggest that the decline towards peak glacial conditions had started by at least 30 ka in the south-eastern Pacific (Lamy et al., 2004; Kaiser et al., 2005; Lamy et al., 2007; Caniupán et al., 2011; Figure 8F and G), west of New Zealand and south of Australia (Pelejero et al., 2006; Barrows et al., 2007a; Calvo et al., 2007; Figure 8E), the Indian Ocean (Labeyrie et al., 1996), and the southeast Atlantic (Barker et al., 2009). A reconstruction from south of the Polar Front also shows a marked increase in Antarctic sea ice between *ca*. 32 and 21 ka, at least in the Atlantic sector of the Southern Ocean (Crosta et al., 2004; Allen et al., 2011), correlating with a reduction in

upwelling (Anderson et al., 2009), which reached a minimum in the last glacial cycle at 30 ka (Figure 8H).

Southern Hemisphere insolation and seasonality both decreased between *ca*. 45 ka and 30 ka, and there was a switch to more rapidly increasing winter duration from *ca*. 36 ka (Huybers & Denton, 2008) that correlates with the timing of culmination of glacial advances in both regions (Figure 7). Terrestrial records complement the evidence for an advance in New Zealand at around 32.7 ka, but do not obviously record earlier advances in New Zealand and Patagonia during late MIS 3. For example, reduced growth in New Zealand speleothems suggest a cooler period from 33 ka into the gLGM (Williams et al., 2015), and the Potrok Aike site in southern Patagonia shows maximum lake levels by 34 ka, indicative of glacial conditions (Hahn et al., 2013; Kliem et al., 2013) and complemented by increasing magnetic susceptibility after *ca*. 32 ka (Lisé-Pronovost et al., 2015). In short, climatic conditions in the southern mid-latitudes were well suited for glacial advances during late MIS 3, although advances during the earlier part of the period show a stronger correlation with insolation variability than with proxy records.

4.1.6 MIS 2 (ca. 29-14 ka) and the gLGM period (26.5-19 ka)

There were clear glacial advances during MIS 2, with peaks marking the onset of retreat either side of the gLGM at 26.9 ka and 18.8 ka in Patagonia and 26.6 ka and 18.1 ka in New Zealand. These correlate with a large (>5%) peak in IRD off the southwest coast of Patagonia, centred on 27 ka and matching a Patagonian glacial advance at that time (Caniupán et al., 2011; Figure 8L). The data also correlate with a significant increase in dust flux in the EDML and EDC ice cores during early MIS 2 (Fischer et al., 2007; Figure 8K and L). Whilst dust levels remained relatively high, IRD reduced markedly through the gLGM, perhaps due to retreating marine-terminating glaciers (Caniupán et al., 2011). Summer insolation increased and peaked at around 21 ka, and seasonality increased, with a latitudinal offset from *ca*. 30 ka (Figure 7). Broadly speaking, the EDML, EDC and Byrd ice cores (Blunier & Brook, 2001; EPICA, 2004, 2006) and NGRIP ice core from Greenland (Rasmussen et al., 2006), demonstrate peak cooling during MIS 2 (and specifically during the gLGM). The onset of glacial retreat occurred at the start and end of a period of intense cooling in Antarctica and Greenland, when significant millennial-scale variability ceased in Antarctica (EPICA, 2006; Rasmussen et al., 2006; Figure 8B and C). Thus, many of the glaciers may have responded rapidly to a drop in Southern Hemisphere temperatures at around 27.5 ka, perhaps because they had already advanced during late MIS 3.

Local SST records around Patagonia show a continuation of the cooler temperatures from late MIS 3 (Lamy et al., 2004; Kaiser et al., 2005), although proximal ice melt off the west coast of southern Patagonia may have caused enhanced cooling of surface waters (Caniupán et al., 2011; Figure 8F). SST changes off the west coast of New Zealand demonstrate the culmination of a cooling trend from MIS 3 into the gLGM (Figure 8E), after which SSTs warmed in both regions. Reconstructions from south of the Polar Front suggest that Antarctic sea ice duration in the southwest Atlantic was at its greatest during the last glacial cycle between *ca*. 32 and 22 ka, consistent with decreasing temperatures in Antarctica (Gersonde, 2003; Allen et al., 2011; Crosta et al., 2004). Maximum summer sea ice retreated to south of 61°S by *ca*. 22 ka, although winter sea ice did not retreat until *ca*. 19 ka, causing a large expanse of seasonally open waters within the Scotia Sea from 22 ka onwards (Allen et al., 2011). Concurrent with this change was an associated increase in upwelling after *ca*. 20 ka (Anderson et al., 2009).

Terrestrially, magnetic susceptibility from Potrok Aike shows a significant increase during the gLGM (Lisé-Pronovost et al., 2015), and speleothem records from New Zealand suggest cooler periods from 33 ka into the gLGM and particularly wet conditions at around 24.7 ka (Williams et al., 2015). Barrell et al. (2013) suggested that full glacial conditions may have begun around 28.8 ka based on a large increase in herb pollen around this time (Vandergoes et al., 2005). Climatic amelioration occurred around 18 ka, based on pollen assemblages and speleothem records (Williams et al., 2015). Overall, in contrast to the Northern Hemisphere (Clark et al., 2009), conditions in the southern mid-latitudes during much of MIS 2 do not seem to have been as well suited for glacial advances compared to late MIS 3: summer insolation and seasonality increased; winter duration decreased; local SSTs decreased little; and IRD, dust flux and Antarctic sea-ice reduced through the period. It is possible that the Southern Hemisphere glacial advances were driven by global temperatures reaching a minimum around the gLGM, driven dominantly by Northern Hemisphere forcing (Clark et al., 2009). Indeed, SSTs in the western Pacific, Indian and Southern Oceans reached a minimum at this time (Barrows & Juggins, 2005). One issue is that many proxy records mitigate against a climatic reversal in Patagonia and New Zealand around 18-19 ka, but glacial advances or still stands clearly occurred at this time.

4.1.7 gLGM to Holocene (ca. 19-10 ka)

Our compilation suggests that glacial advances culminated at 13.9 ka in Patagonia and 13.0 ka in New Zealand, during the Antarctic Cold Reversal (*ca*. 14.5-12.9 ka; Jouzel et al., 2001) rather than the Younger Dryas cold period in the North Atlantic (*ca*. 12.9-11.7 ka;

Rasmussen et al., 2006; Lowe et al., 2008). An absence of evidence for changes in the IRD or dust records may imply that the advance was either weak or, more probably, a prolonged still stand (Figure 8K and L). Antarctic temperatures decreased at this time (Figure 8B and C), in anti-phase with a warm period in Greenland, so that the event was prior to the Younger Dryas (EPICA, 2006; Rasmussen et al., 2006). This temperature drop only registers as a plateau in overall warming in the local SST records (Caniupán et al., 2011), consistent with a minimal advance of glaciers at this time. Southern Hemisphere insolation was decreasing (Berger & Loutre, 1991), but the sub-orbital timescale of the events suggests that they were not likely related to changes in insolation intensity (Figure 7). There was an apparent drop in upwelling (Anderson et al., 2009; Figure 8I), which could indicate northern migration of the Southern Westerly Winds and oceanic fronts, triggering a slowdown in the recession of glaciers in Patagonia and New Zealand.

4.2 The cause of glacial advances

The evidence from our dating compilation shows that glacial advances culminated at various times during the last glacial cycle, with some major advances occurring prior to the gLGM and some advances in Patagonia and New Zealand culminating *broadly* synchronously. We now consider the possible forcing factors controlling glacial activity, including the reasons for the offsets in timing between Patagonia and New Zealand glaciers. Previous studies have focussed on insolation variability and shifts in atmospheric and/or oceanic frontal systems as the most likely controls on glacial activity. These include summer insolation; winter duration; seasonality; the migration of the Sub-Antarctic and Sub-tropical fronts; and the shifting of the Southern Westerly Winds. Antarctic sea ice and Southern Ocean stratification may also have triggered feedbacks within the climate system. Determining which of these systems is important is complex, and the forcing factors may have changed between glacial advances.

4.2.1 Insolation changes

The expansion of large ice sheets in the Northern Hemisphere broadly followed decreases in summer insolation intensity (Figure 7). There are two conundrums associated with this model in the Southern Hemisphere. The first is that many Southern Hemisphere climate proxies, including Antarctic temperature records, suggest glacial-interglacial climate change occurred broadly in-phase between the Southern and Northern Hemispheres, despite covariance of summer insolation (Mercer, 1984; Jouzel et al., 2007; Wolff et al., 2010a; Huybers & Denton, 2008). Secondly, glacial activity prior to the gLGM, as observed in our

compiled chronology, is at odds with a model in which conditions suited to maximum ice growth occurred during the gLGM (Barrows et al., 2007a; Wolff et al., 2009; Doughty et al., 2015). One explanation is that, for the Southern Hemisphere, the duration of seasons may exert a greater control on climate than insolation intensity (Huybers & Denton, 2008). Increasing southern winter duration, synchronous with decreasing northern summer insolation, could explain why broad glacial-interglacial changes in both hemispheres occurred at the same time (Putnam et al., 2013b; Figure 7C). Winter duration may also explain why glacial culminations in the southern mid-latitudes occurred prior to the gLGM, given that there was a trend toward longer winters during MIS 3 and into MIS 2 (Huybers & Denton, 2008). Furthermore, reduced seasonality might also have promoted ice mass growth (taken here as times of cooler summers and warmer winters; Figure 7E).

Doughty et al. (2015) noted that activity of the Pukaki glacier in New Zealand showed no consistent relationship with Southern Hemisphere insolation. Our compilation shows a pattern between the timing of glacial activity in Patagonia and New Zealand and the broad overlap in insolation minima between the Northern and Southern Hemispheres (Figure 7F-I). However, like Doughty et al. (2015), we find that culminations in advances in both regions occurred during both the rising and falling limbs of insolation change (Figure 7D, J and K). Consequently, we suggest that whilst weaker Southern Hemisphere insolation may have established temperature conditions that primed glaciers for advances, it is unlikely to have been the primary forcing factor.

4.2.2 Atmospheric and sea surface temperature changes

Warming events in the Antarctic ice cores during MIS 4 and MIS 3 (A1-4; Blunier & Brook, 2001) have been correlated across the southern mid-latitudes (Lamy et al., 2004; Barrows et al., 2007a; Kelley et al., 2014; Figure 8D). Additional Antarctic Isotope Maxima (AIM) events, identified in the EDML ice core (EPICA, 2006; Figure 8B), broadly coincide with Dansgaard-Oeschger events in NGRIP. However, both ice core and SST records show a lead in the Southern Hemisphere during the last glacial cycle (EPICA, 2006; Wolff et al., 2009). The propagation of Antarctic temperature changes through the atmosphere has been advocated as a trigger for glacial advances in the southern mid-latitudes (Kelley et al., 2014), and there seems to be a link between the onset of minimum temperatures recorded in Antarctica at the start of MIS 2 (Figure 8B and C) and the glacial culminations we identify at 26-27 ka (Figure 8M and N). Whilst individual glacial records may align with temperature minima in Antarctica (e.g. Kelley et al., 2014), our compilation does not show a clear, consistent pattern between Antarctic events and glacial activity.

Millennial-scale events recorded in mid-latitude SST records likely reflect changes in the position of oceanic fronts (Barrows et al., 2007a). The migration of the Sub-Tropical Front and Sub-Antarctic Front over time would have altered SSTs around Patagonia and New Zealand by altering heat-transfer flows such as the Agulhas Current off southern Africa (Barrows et al., 2007a) and the position and/or intensity of the Antarctic Circumpolar Current and Southern Westerly Wind system, whilst also influencing latitudinal SST gradients (Shulmeister et al., 2004; Kaiser et al., 2005). Lamy et al. (2007) and Denton et al. (2010) considered a coupled atmosphere-ocean system in which latitudinal shifts in the Sub-Tropical Front and Southern Westerly Winds occurred in response to changes in the Inter-Tropical Convergence Zone, driven by Northern Hemisphere sea ice extent, and changes in the sea ice extent around Antarctica. Several records suggest northward migration of oceanic fronts during globally-cooler periods that resulted in reduced SSTs around Patagonia and New Zealand. In the southwest and central Pacific, the Sub-Tropical Front may have migrated 1-2° (Sikes et al., 2009) or more (Barrows et al., 2000), whilst in the southeast Pacific the Sub-Tropical Front and Sub-Antarctic Front may have shifted substantially, possibly as much as 5-6° during MIS 2 (Gersonde et al., 2005; Kaiser et al., 2005; Caniupán et al., 2011). The effect on SSTs in northern Patagonia and New Zealand (Lamy et al., 2004; Barrows et al., 2007a; Figure 8E and F) compared to southern Patagonia (Caniupán et al., 2011; Figure 8G) supports the role of a coupled oceanic-atmospheric frontal system, rather than hemisphere-wide cooling. It is also possible that the migration of the Southern Westerly Winds, followed by the oceanic fronts, may explain the offset in glacial timing between Patagonia and New Zealand at 26-27 ka, 18-19 ka and 13-14 ka, given that higher latitude glaciers would have responded first to a northward migration of precipitation and temperature. However, the reason that Patagonian advances culminated prior to those in New Zealand is less clear. Notwithstanding this uncertainty, the shifting of fronts in both regions would have resulted in reasonably rapid increases in precipitation followed by changes in local temperatures, triggering terrestrial cooling and glacial advances.

The migration of a coupled atmosphere-ocean system is sufficient to explain most of the glacial patterns in our compilation, and is broadly supported by SST records. A key exception are the advances culminating at 18-19 ka, when SSTs west of Patagonia decreased (Figure 8F and G), but SSTs west of New Zealand increased (Figure 8E) and Antarctic temperatures suggest warming (Figure 8B-D). Furthermore, terrestrial proxy records such as grass pollen in Patagonia (Heusser et al., 1999), and forest pollen (Ryan et al., 2012; Vandergoes et al., 2013) and speleothem records in New Zealand (Williams et al., 2015), indicate climatic amelioration at this time. The glacial activity in Patagonia may be

linked to a regional drop in SST, but the reason for similar activity in New Zealand is unclear, and we are not yet able to establish a satisfactory mechanism that can account for the culmination of advances in both regions, despite differing regional SST records.

4.2.3 The role of sea ice and ocean stratification

A critical component of a coupled atmosphere-ocean system as a control on southern mid-latitude glacial activity is the role of sea ice and oceanic upwelling on the stratification of the Southern Ocean. Antarctic sea ice has been invoked in several explanations for global climate change during the last glacial cycle (Allen et al., 2011). It is likely that seasonally-expanded sea ice would have increased deep water formation and expansion (Seidov & Maslin, 2001; Ferrari et al., 2014) and promoted stratification of the Southern Ocean due to freshening of the surface waters (Putnam et al., 2013b). Sea-ice extent is also likely to have been reduced by a southward shift of the Southern Westerly Winds and oceanic fronts, helping to destabilise any stratification of the Southern Ocean. There is, then, a potentially important link between Antarctic sea ice and global glacial-interglacial climate change (Denton et al., 2010), and an intrinsic link between sea ice and Southern Ocean stratification (Putnam et al., 2013b).

The Southern Ocean may have entered a fully stratified state by *ca*. 70 ka (Anderson et al., 2009; Figure 8H), consistent with the build-up of Antarctic sea ice at this time (Crosta et al., 2004; Figure 8J), and possibly linked to increased winter duration (Putnam et al., 2013b). Greater sea ice extent would have promoted stratification and forced the Southern Ocean fronts northward, increasing SST gradients so that the Southern Westerly Winds also migrated north. Migration of the winds may have enhanced sea ice growth, creating a positive feedback. This model, advocated by Denton et al. (2010) and Putnam et al. (2013), amongst others, provides a theoretical link between sea ice formation, Sub-Tropical front and Sub-Antarctic Front migration, Southern Westerly Wind migration, and SST changes around Patagonia and New Zealand. However, until more detailed and spatially-extensive records of sea-ice and upwelling have been produced, it is difficult to ascertain whether these factors lead or lag changes in the climatic system.

5 Conclusions

The first compilation of previously published ^{10}Be exposure dating for Patagonia and New Zealand suggests that glacial advances culminated at various times throughout the last

glacial cycle. There is commonality in the timing of glacial activity between numerous glaciers in both Patagonia and New Zealand, and we infer this to represent periods of broad, regional glacial advances. However, this does not mean that *all* glaciers advanced and retreated synchronously and does not necessarily provide information on the extent of the glacial activity. That said, it is clear that the chronologies from Patagonia and New Zealand show remarkable similarities, suggesting that similar forcing factors may have influenced both ice masses during the last glacial cycle. In particular, both regions show a trend for glacial activity, replicated by different glaciers, from at least 45 ka, with culminations in either region at 41.3 ka, 37.8 ka and 32.7 ka, and in both regions at *ca*. 26-27 ka, 18-19 ka and 13-14 ka.

Our compilation reveals a number of significant characteristics in the timing of glacial activity in the southern mid-latitudes. Glaciers were advancing by the latter half of MIS 3, well before the gLGM, with clear evidence of advances culminating prior to 30 ka. Further advances culminated just before and after the gLGM and during the Antarctic Cold Reversal. Future work should target glacial limits down-ice of those dated to the gLGM, particularly in Patagonia, where there are substantially fewer exposure ages. In particular, a general absence of dated limits from MIS 4 is puzzling given that numerous proxy records suggest that this period resulted in significant climate deterioration in the southern mid-latitudes. A well dated limit of the Pukaki glacier at this time may indicate that other, similar glacial limits have not yet been sampled.

There is no clear correlation between a single climatic forcing factor and the glacial activity from our compilation. Rather, the forcing factors responsible likely varied over time. Glacial advances may have been paced by underlying orbital parameters, but insolation changes alone cannot explain their timing. Our study suggests that ice expansion was broadly synchronous between Patagonia and New Zealand, implying that the forcing factors involved coherent zonal fluctuations of the oceanic fronts and/or southern westerly winds. Late MIS 3 likely experienced optimum conditions for glacial activity in the southern mid-latitudes, despite preceding the coolest temperatures in Antarctica. Summer insolation reached a minimum, seasonality was reduced, winter duration was increasing, and sea ice had expanded significantly. Such conditions may have induced stratification of the ocean and an equatorward shift in the moisture-bearing Southern Westerly Winds, delivering greater precipitation to Patagonia and New Zealand prior to colder temperatures as the Sub-tropical Front and Sub-Antarctic Front migrated northwards.

Whilst global temperatures did not reach a minimum until MIS 2, summer insolation in the Southern Hemisphere was greater by that time, and Antarctic sea ice had reduced markedly.

Glacial advances during MIS 2 in Patagonia and New Zealand occurred rapidly with the onset of a prolonged cool phase across the gLGM, marked by a discontinuation of hemispheric millennial-scale variability. A consistent offset in the timing of glacial activity after 30 ka, in which Patagonian glaciers began retreating before those in New Zealand, is unlikely to be an artefact of age calculation. The offset could instead relate to the latitudinal migration of the coupled ocean-atmosphere system or a latitudinal offset in seasonality from *ca*. 30 ka. The implication is that our dataset not only suggests that glaciers in Patagonia and New Zealand advanced and retreated at different times to the large Northern Hemisphere ice sheets, but that this activity was the result of major rearrangements of the Southern Hemisphere climate system during the last glacial cycle. Such rearrangements would have altered the position and intensity of the Southern Westerly Winds and oceanic fronts, as well as wind-driven upwelling of the deep Southern Ocean. To conclude, glacial activity during the last glacial cycle in Patagonia and New Zealand responded primarily to oceanic and atmospheric feedbacks in the Southern Hemisphere climate system paced by underlying orbital forcing.

6 Acknowledgments

This research was funded by a UK NERC Ph.D. studentship (NE/j500215/1) awarded to CMD at Durham University. We are grateful to Dave Evans and Neil Glasser for their comments on an earlier version of the manuscript. We thank two anonymous reviewers and Tim Barrows for their critical and comprehensive reviews of the manuscript, and Neil Glasser for his editorial work throughout.

7 Supplementary data

Included with this paper is a supplementary figure that shows the New Zealand Rakaia sequence and a spreadsheet containing the raw data from Patagonia and New Zealand.

8 References

Ackert, R.P., Becker, R.A., Singer, B.S., Kurz, M.D., Caffee, M.W. & Mickelson, D.M. (2008). Patagonian Glacier Response During the Late Glacial–Holocene Transition. *Science* **321** (5887), 392–395.

Allen, C.S., Pike, J. & Pudsey, C.J. (2011). Last glacial-interglacial sea-ice cover in the SW Atlantic and its potential role in global deglaciation. *Quaternary Science Reviews* **30** (19-20), 2446–2458.

Anderson, R.F., Ali, S., Bradtmiller, L.I., Nielsen, S.H.H., Fleisher, M.Q., Anderson, B.E. & Burckle, L.H. (2009). Wind-Driven Upwelling in the Southern Ocean and the Deglacial Rise in Atmospheric CO2. *Science* **323** (5920), 1443–1448.

Applegate, P.J., Urban, N.M., Laabs, B.J.C., Keller, K. & Alley, R.B. (2010). Modeling the statistical distributions of cosmogenic exposure dates from moraines. *Geoscientific Model Development* **3**, 293–307.

Barker, S., Diz, P., Vautravers, M.J., Pike, J., Knorr, G., Hall, I.R. & Broecker, W.S. (2009). Interhemispheric Atlantic seesaw response during the last deglaciation. *Nature* **457** (7233), 1097–1102.

Barrell, D.J.A. (2011). Quaternary Glaciers of New Zealand. In: J. Ehlers, P. L. Gibbard, & P. D. Hughes (eds.). *Developments in Quaternary Sciences*. Developments in Quaternary Sciences. **15**, 1047–1064, Elsevier.

Barrell, D.J.A., Almond, P.C., Vandergoes, M.J., Lowe, D.J. & Newnham, R.M. (2013). A composite pollen-based stratotype for inter-regional evaluation of climatic events in New Zealand over the past 30,000 years (NZ-INTIMATE project). *Quaternary Science Reviews* **74**, 4–20.

Barrows, T.T., Almond, P.C., Rose, R., Keith Fifield, L., Mills, S.C., Tims, S.G., Barrell, D.J.A., Almond, P.C., Vandergoes, M.J., Lowe, D.J., Newnham, R.M., Barrows, T.T., Almond, P.C., Rose, R., Keith Fifield, L., Mills, S.C., Tims, S.G., Juggins, S., De Deckker, P., Calvo, E. & Pelejero, C. (2013). Late Pleistocene glacial stratigraphy of the Kumara-Moana region, West Coast of South Island, New Zealand. *Quaternary Science Reviews* **74** (2), 139–159.

Barrows, T.T. & Juggins, S. (2005). Sea-surface temperatures around the Australian margin and Indian Ocean during the Last Glacial Maximum. *Quaternary Science Reviews* **24** (7-9), 1017–1047.

Barrows, T.T., Juggins, S., De Deckker, P., Calvo, E. & Pelejero, C. (2007a). Long-term sea surface temperature and climate change in the Australian-New Zealand region. *Paleoceanography* **22** (2), n/a–n/a.

Barrows, T.T., Juggins, S., De Deckker, P., Thiede, J. & Martinez, J.I. (2000). Sea-surface temperatures of the southwest Pacific Ocean during the Last Glacial Maximum. *Paleoceanography* **15** (1), 95–109.

Barrows, T.T., Lehman, S.J., Fifield, L.K. & De Deckker, P. (2007b). Absence of Cooling in New Zealand and the Adjacent Ocean During the Younger Dryas Chronozone. *Science* **318** (5847), 86–89.

Barrows, T.T., Stone, J.O., Fifield, L.K. & Cresswell, R.G. (2002). The timing of the Last Glacial Maximum in Australia. *Quaternary Science Reviews* **21** (1–3), 159–173.

Berger, A. & Loutre, M.F. (1991). Insolation values for the climate of the last 10 million years. *Quaternary Science Reviews* **10** (4), 297–317.

Blunier, T. & Brook, E.J. (2001). Timing of Millennial-Scale Climate Change in Antarctica and

Greenland During the Last Glacial Period. *Science* **291** (5501), 109–112.

Brown, E., Colling, A., Park, D., Phillips, J., Rothery, D. & Wright, J. (2001). *Ocean Circulation*. 2nd Ed. [Online]. Oxford: Butterworth-Heinemann; Open University.

Calvo, E., Pelejero, C., De Deckker, P. & Logan, G.A. (2007). Antarctic deglacial pattern in a 30 kyr record of sea surface temperature offshore South Australia. *Geophysical Research Letters* **34** (13), n/a–n/a.

Caniupán, M., Lamy, F., Lange, C.B., Kaiser, J., Arz, H., Kilian, R., Baeza Urrea, O., Aracena, C., Hebbeln, D., Kissel, C., Laj, C., Mollenhauer, G. & Tiedemann, R. (2011). Millennial-scale sea surface temperature and Patagonian Ice Sheet changes off southernmost Chile (53°S) over the past 60 kyr. *Paleoceanography* **26** (3), n/a–n/a.

Carter, L., McCave, I.N. & Williams, M.J.M. (2008). Circulation and Water Masses of the Southern Ocean: A Review F. Fabio & S. Martin (eds.). *Developments in Earth and Environmental Sciences* **8** (08), 85–114.

Clark, P.U., Clague, J.J., Curry, B.B., Dreimanis, A., Hicock, S.R., Miller, G.H., Berger, G.W., Eyles, N., Lamothe, M., Miller, B.B., Mott, R.J., Oldale, R.N., Stea, R.R., Szabo, J.P., Thorleifson, L.H. & Vincent, J.-S. (1993). Initiation and development of the Laurentide and Cordilleran Ice Sheets following the last interglaciation. *Quaternary Science Reviews* **12** (2), 79–114.

Clark, P.U., Dyke, A.S., Shakun, J.D., Carlson, A.E., Clark, J., Wohlfarth, B., Mitrovica, J.X., Hostetler, S.W. & McCabe, A.M. (2009). The Last Glacial Maximum. *Science* **325** (5941), 710–714.

Coronato, A. & Rabassa, J. (2011). Pleistocene Glaciations in Southern Patagonia and Tierra del Fuego. In: J. Ehlers, P. L. Gibbard, & P. D. Hughes (eds.). *Developments in Quaternary Sciences*. **15**, 715–727, Elsevier.

Crosta, X., Sturm, A., Armand, L. & Pichon, J.-J. (2004). Late Quaternary sea ice history in the Indian sector of the Southern Ocean as recorded by diatom assemblages. *Marine Micropaleontology* **50** (3-4), 209–223.

Darvill, C.M., Bentley, M.J., Stokes, C.R., Hein, A.S. & Rodés, Á. (2015). Extensive MIS 3 glaciation in southernmost Patagonia revealed by cosmogenic nuclide dating of outwash sediments. *Earth and Planetary Science Letters* **429**, 157–169.

Denton, G.H., Anderson, R.F., Toggweiler, J.R., Edwards, R.L., Schaefer, J.M. & Putnam, A.E. (2010). The Last Glacial Termination. *Science* **328** (5986), 1652–1656.

Denton, G.H., Lowell, T. V, Heusser, C.J., Schlüchter, C., Andersen, B.G., Heusser, L.E., Moreno, P.I. & Marchant, D.R. (1999). Geomorphology, Stratigraphy, and Radiocarbon Chronology of LlanquihueDrift in the Area of the Southern Lake District, Seno Reloncaví, and Isla Grande de Chiloé, Chile. *Geografiska Annaler: Series A, Physical Geography* **81** (2), 167–229.

Desilets, D., Zreda, M. & Prabu, T. (2006). Extended scaling factors for in situ cosmogenic nuclides: New measurements at low latitude. *Earth and Planetary Science Letters* **246** (3–4), 265–276.

Doughty, A.M., Schaefer, J.M., Putnam, A.E., Denton, G.H., Kaplan, M.R., Barrell, D.J.A., Andersen, B.G., Kelley, S.E., Finkel, R.C. & Schwartz, R. (2015). Mismatch of glacier extent and summer insolation in Southern Hemisphere mid-latitudes. *Geology* **43** (5), 407–410.

Douglass, D.C., Singer, B.S., Kaplan, M.R., Ackert, R.P., Mickelson, D.M. & Caffee, M.W. (2005). Evidence of early Holocene glacial advances in southern South America from cosmogenic surface-exposure dating. *Geology* **33** (3), 237–240.

Douglass, D.C., Singer, B.S., Kaplan, M.R., Mickelson, D.M. & Caffee, M.W. (2006). Cosmogenic nuclide surface exposure dating of boulders on last-glacial and late-glacial moraines, Lago Buenos Aires, Argentina: Interpretive strategies and paleoclimate implications. *Quaternary Geochronology* **1** (1), 43–58.

Dunai, T.J. (2001). Influence of secular variation of the geomagnetic field on production rates of in situ produced cosmogenic nuclides. *Earth and Planetary Science Letters* **193** (1–2), 197–212.

EPICA (2004). Eight glacial cycles from an Antarctic ice core. *Nature* **429** (6992), 623–628.

EPICA (2006). One-to-one coupling of glacial climate variability in Greenland and Antarctica. *Nature* **444** (7116), 195–198.

Evenson, E.B., Burkhart, P.A., Gosse, J.C., Baker, G.S., Jackofsky, D., Meglioli, A., Dalziel, I., Kraus, S., Alley, R.B. & Berti, C. (2009). Enigmatic boulder trains, supraglacial rock avalanches, and the origin of 'Darwin's boulders,' Tierra del Fuego. *GSA Today* **19** (12), 4–10.

Ferrari, R., Jansen, M.F., Adkins, J.F., Burke, A., Stewart, A.L. & Thompson, A.F. (2014). Antarctic sea ice control on ocean circulation in present and glacial climates. *Proceedings of the National Academy of Sciences of the United States of America* **111** (24), 8753–8.

Fischer, H., Fundel, F., Ruth, U., Twarloh, B., Wegner, A., Udisti, R., Becagli, S., Castellano, E., Morganti, A., Severi, M., Wolff, E., Littot, G., Röthlisberger, R., Mulvaney, R., Hutterli, M.A., Kaufmann, P., Federer, U., Lambert, F., Bigler, M., Hansson, M., Jonsell, U., de Angelis, M., Boutron, C., Siggaard-Andersen, M.-L., Steffensen, J.P., Barbante, C., Gaspari, V., Gabrielli, P. & Wagenbach, D. (2007). Reconstruction of millennial changes in dust emission, transport and regional sea ice coverage using the deep EPICA ice cores from the Atlantic and Indian Ocean sector of Antarctica. *Earth and Planetary Science Letters* **260** (1–2), 340–354.

Fogwill, C.J. (2003). *The application of cosmogenic exposure dating to glacial landforms: Examples from Antarctica and Patagonia*. University of Edinburgh.

Fogwill, C.J. & Kubik, P.W. (2005). A glacial stage spanning the Antarctic Cold Reversal in Torres del Paine (51 degrees S), Chile, based on preliminary cosmogenic exposure ages. *Geografiska Annaler Series a-Physical Geography* **87A** (2), 403–408.

García, J.L., Kaplan, M.R., Hall, B.L., Schaefer, J.M., Vega, R.M., Schwartz, R. & Finkel, R. (2012). Glacier expansion in southern Patagonia throughout the Antarctic cold reversal. *Geology* **40**, 859–862.

Gersonde, R. (2003). Last glacial sea surface temperatures and sea-ice extent in the Southern Ocean (Atlantic-Indian sector): A multiproxy approach. *Paleoceanography* **18** (3), 1061.

Gersonde, R., Crosta, X., Abelmann, A. & Armand, L. (2005). Sea-surface temperature and sea ice distribution of the Southern Ocean at the EPILOG Last Glacial Maximum—a circum-Antarctic view based on siliceous microfossil records. *Quaternary Science Reviews* **24** (7-9), 869–896.

Glasser, N.F., Harrison, S., Ivy-Ochs, S., Duller, G.A.T. & Kubik, P.W. (2006). Evidence from the Rio Bayo valley on the extent of the North Patagonian Icefield during the Late Pleistocene–Holocene transition. *Quaternary Research* **65** (1), 70–77.

Glasser, N.F., Harrison, S., Schnabel, C., Fabel, D. & Jansson, K.N. (2012). Younger Dryas and early Holocene age glacier advances in Patagonia. *Quaternary Science Reviews* **58** (0), 7–17.

Glasser, N.F., Jansson, K.N., Goodfellow, B.W., de Angelis, H., Rodnight, H. & Rood, D.H. (2011). Cosmogenic nuclide exposure ages for moraines in the Lago San Martín Valley, Argentina. *Quaternary Research* **75** (3), 636–646.

Hahn, A., Kliem, P., Ohlendorf, C., Zolitschka, B. & Rosén, P. (2013). Climate induced changes as registered in inorganic and organic sediment components from Laguna Potrok Aike (Argentina) during the past 51 ka. *Quaternary Science Reviews* **71**, 154–166.

Hein, A.S., Dunai, T.J., Hulton, N.R.J. & Xu, S. (2011). Exposure dating outwash gravels to determine the age of the greatest Patagonian glaciations. *Geology* **39** (2), 103–106.

Hein, A.S., Hulton, N.R.J., Dunai, T.J., Schnabel, C., Kaplan, M.R., Naylor, M. & Xu, S. (2009). Middle Pleistocene glaciation in Patagonia dated by cosmogenic-nuclide measurements on outwash gravels. *Earth and Planetary Science Letters* **286** (1-2), 184–197.

Hein, A.S., Hulton, N.R.J., Dunai, T.J., Sugden, D.E., Kaplan, M.R. & Xu, S. (2010). The chronology of the Last Glacial Maximum and deglacial events in central Argentine Patagonia. *Quaternary Science Reviews* **29** (9-10), 1212–1227.

Heusser, C.J., Heusser, L.E. & Lowell, T. V. (1999). Paleoecology of The Southern Chilean Lake District-Isla Grande de Chiloe During Middle-late Llanquihue Glaciation and Deglaciation. *Geografiska Annaler, Series A: Physical Geography* **81** (2), 231–284.

Hughes, P.D., Gibbard, P.L. & Ehlers, J. (2013). Timing of glaciation during the last glacial cycle: evaluating the concept of a global 'Last Glacial Maximum' (LGM). *Earth-Science Reviews* **125**, 171–198.

Huybers, P. & Denton, G. (2008). Antarctic temperature at orbital timescales controlled by local summer duration. *Nature Geosci* **1** (11), 787–792.

Ivy-Ochs, S., Schluchter, C., Kubik, P.W., Denton, G.H., Schlüchter, C., Kubik, P.W. & Denton, G.H. (1999). Moraine Exposure Dates Imply Synchronous Younger Dryas Glacier Advances in the European Alps and in the Southern Alps of New Zealand. *Geografiska Annaler: Series A, Physical Geography* **81A** (2), 313–323.

Jouzel, J., Masson, V., Cattani, O., Falourd, S., Stievenard, M., Stenni, B., Longinelli, A., Johnsen, S.J., Steffenssen, J.P., Petit, J.R., Schwander, J., Souchez, R. & Barkov, N.I. (2001). A new 27 ky high resolution East Antarctic climate record. *Geophysical Research Letters* **28** (16), 3199–3202.

Jouzel, J., Masson-Delmotte, V., Cattani, O., Dreyfus, G., Falourd, S., Hoffmann, G., Minster, B., Nouet, J., Barnola, J.M., Chappellaz, J., Fischer, H., Gallet, J.C., Johnsen, S., Leuenberger, M., Loulergue, L., Luethi, D., Oerter, H., Parrenin, F., Raisbeck, G., Raynaud, D., Schilt, A., Schwander, J., Selmo, E., Souchez, R., Spahni, R., Stauffer, B., Steffensen, J.P., Stenni, B., Stocker, T.F., Tison, J.L., Werner, M. & Wolff, E.W. (2007). Orbital and millennial Antarctic climate variability over the past 800,000 years. *Science* **317** (5839), 793–6.

Kaiser, J. & Lamy, F. (2010). Links between Patagonian Ice Sheet fluctuations and Antarctic dust variability during the last glacial period (MIS 4-2). *Quaternary Science Reviews* **29** (11–12), 1464–1471.

Kaiser, J., Lamy, F. & Hebbeln, D. (2005). A 70-kyr sea surface temperature record off southern Chile (Ocean Drilling Program Site 1233). *Paleoceanography* **20** (4), n/a–n/a.

Kaplan, M.R., Ackert, R.P., Singer, B.S., Douglass, D.C. & Kurz, M.D. (2004). Cosmogenic nuclide chronology of millennial-scale glacial advances during O-isotope stage 2 in Patagonia. *Geological Society of America Bulletin* **116** (3-4), 308–321.

Kaplan, M.R., Coronato, A., Hulton, N.R.J., Rabassa, J.O., Kubik, P.W. & Freeman, S.P.H.T. (2007). Cosmogenic nuclide measurements in southernmost South America and implications for landscape change. *Geomorphology* **87** (4), 284–301.

Kaplan, M.R., Douglass, D.C., Singer, B.S. & Caffee, M.W. (2005). Cosmogenic nuclide chronology of pre-last glacial maximum moraines at Lago Buenos Aires, 46°S, Argentina. *Quaternary Research* **63** (3), 301–315.

Kaplan, M.R., Fogwill, C.J., Sugden, D.E., Hulton, N., Kubik, P.W. & Freeman, S.P.H.T. (2008). Southern Patagonian glacial chronology for the Last Glacial period and implications for Southern Ocean climate. *Quaternary Science Reviews* **27** (3-4), 284–294.

Kaplan, M.R., Schaefer, J.M., Denton, G.H., Barrell, D.J.A., Chinn, T.J.H., Putnam, A.E., Andersen, B.G., Finkel, R.C., Schwartz, R. & Doughty, A.M. (2010). Glacier retreat in New Zealand during the Younger Dryas stadial. *Nature* **467** (7312), 194–197.

Kaplan, M.R., Schaefer, J.M., Denton, G.H., Doughty, A.M., Barrell, D.J.A., Chinn, T.J.H., Putnam, A.E., Andersen, B.G., Mackintosh, A., Finkel, R.C., Schwartz, R. & Anderson, B. (2013). The anatomy of long-term warming since 15 ka in New Zealand based on net glacier snowline rise. *Geology* **41** (8), 887–890.

Kaplan, M.R., Strelin, J.A., Schaefer, J.M., Denton, G.H., Finkel, R.C., Schwartz, R., Putnam, A.E., Vandergoes, M.J., Goehring, B.M. & Travis, S.G. (2011). In-situ cosmogenic 10Be production rate at Lago Argentino, Patagonia: Implications for late-glacial climate chronology. *Earth and Planetary Science Letters* **309** (1-2), 21–32.

Kelley, S.E., Kaplan, M.R., Schaefer, J.M., Andersen, B.G., Barrell, D.J.A., Putnam, A.E., Denton, G.H., Schwartz, R., Finkel, R.C. & Doughty, A.M. (2014). High-precision 10Be chronology of moraines in the Southern Alps indicates synchronous cooling in Antarctica and New Zealand 42,000 years ago. *Earth and Planetary Science Letters* **405**, 194–206.

Kleman, J., Hättestrand, C., Borgström, I. & Stroeven, A. (1997). Fennoscandian palaeoglaciology reconstructed using a glacial geological inversion model. *Journal of Glaciology* **43** (144), 283–299.

Kliem, P., Buylaert, J.P., Hahn, A., Mayr, C., Murray, A.S., Ohlendorf, C., Veres, D., Wastegård, S. & Zolitschka, B. (2013). Magnitude, geomorphologic response and climate links of lake level oscillations at Laguna Potrok Aike, Patagonian steppe (Argentina). *Quaternary Science Reviews* **71**, 131–146.

Labeyrie, L., Labracherie, M., Gorfti, N., Pichon, J.J., Vautravers, M., Arnold, M., Duplessy, J.-C., Paterne, M., Michel, E., Duprat, J., Caralp, M. & Turon, J.-L. (1996). Hydrographic changes of the Southern Ocean (southeast Indian Sector) Over the last 230 kyr. *Paleoceanography* **11** (1), 57–76.

Lal, D. (1991). Cosmic ray labeling of erosion surfaces: in situ nuclide production rates and erosion models. *Earth and Planetary Science Letters* **104** (2–4), 424–439.

Lamy, F., Kaiser, J., Arz, H.W., Hebbeln, D., Ninnemann, U., Timm, O., Timmermann, A. & Toggweiler, J.R. (2007). Modulation of the bipolar seesaw in the Southeast Pacific during Termination 1. *Earth and Planetary Science Letters* **259** (3–4), 400–413.

Lamy, F., Kaiser, J., Ninnemann, U., Hebbeln, D., Arz, H.W. & Stoner, J. (2004). Antarctic Timing of Surface Water Changes off Chile and Patagonian Ice Sheet Response. *Science* **304** (5679), 1959–1962.

Lifton, N.A., Bieber, J.W., Clem, J.M., Duldig, M.L., Evenson, P., Humble, J.E. & Pyle, R. (2005). Addressing solar modulation and long-term uncertainties in scaling secondary

cosmic rays for in situ cosmogenic nuclide applications. *Earth and Planetary Science Letters* **239** (1–2), 140–161.

Lisé-Pronovost, A., St-Onge, G., Gogorza, C., Haberzettl, T., Jouve, G., Francus, P., Ohlendorf, C., Gebhardt, C. & Zolitschka, B. (2015). Rock-magnetic proxies of wind intensity and dust since 51,200 cal BP from lacustrine sediments of Laguna Potrok Aike, southeastern Patagonia. *Earth and Planetary Science Letters* **411**, 72–86.

Lisiecki, L.E. & Raymo, M.E. (2005). A Pliocene-Pleistocene stack of 57 globally distributed benthic δ18O records. *Paleoceanography* **20** (1), PA1003.

Lowe, J.J., Rasmussen, S.O., Björck, S., Hoek, W.Z., Steffensen, J.P., Walker, M.J.C. & Yu, Z.C. (2008). Synchronisation of palaeoenvironmental events in the North Atlantic region during the Last Termination: a revised protocol recommended by the INTIMATE group. *Quaternary Science Reviews* **27** (1–2), 6–17.

Lüthi, D., Le Floch, M., Bereiter, B., Blunier, T., Barnola, J.-M., Siegenthaler, U., Raynaud, D., Jouzel, J., Fischer, H., Kawamura, K. & Stocker, T.F. (2008). High-resolution carbon dioxide concentration record 650,000-800,000 years before present. *Nature* **453** (7193), 379–82.

McCulloch, R.D., Fogwill, C.J., Sugden, D.E., Bentley, M.J. & Kubik, P.W. (2005). Chronology of the last glaciation in central Strait of Magellan and Bahia Inutil, southernmost South America. *Geografiska Annaler Series a-Physical Geography* **87A** (2), 289–312.

McGee, D., Broecker, W.S. & Winckler, G. (2010). Gustiness: The driver of glacial dustiness? *Quaternary Science Reviews* **29** (17–18), 2340–2350.

Mercer, J.H. (1984). Simultaneous climatic change in both hemispheres and similar bipolar interglacial warming: evidence and implications. In: J. E. Hansen & T. Takahashi (eds.). *Climate Processes and Climate Sensitivity*. Geophysical Monograph Series. **29**, 307–313, Washington, D. C.: American Geophysical Union.

Moreno, P.I., Denton, G.H., Moreno, H., Lowell, T. V., Putnam, A.E. & Kaplan, M.R. (2015). Radiocarbon chronology of the last glacial maximum and its termination in northwestern Patagonia. *Quaternary Science Reviews* **122**, 233–249.

Moreno, P.I., Kaplan, M.R., Francois, J.P., Villa-Martinez, R., Moy, C.M., Stern, C.R. & Kubik, P.W. (2009). Renewed glacial activity during the Antarctic cold reversal and persistence of cold conditions until 11.5 ka in southwestern Patagonia. *Geology* **37** (4), 375–378.

Murray, D.S., Carlson, A.E., Singer, B.S., Anslow, F.S., He, F., Caffee, M., Marcott, S.A., Liu, Z. & Otto-Bliesner, B.L. (2012). Northern Hemisphere forcing of the last deglaciation in southern Patagonia. *Geology* **40**, 631–634.

Orsi, A.H., Whitworth, T. & Nowlin, W.D. (1995). On the meridional extent and fronts of the Antarctic Circumpolar Current. *Deep Sea Research Part I: Oceanographic Research Papers* **42** (5), 641–673.

Pelejero, C., Calvo, E., Barrows, T.T., Logan, G.A. & De Deckker, P. (2006). South Tasman Sea alkenone palaeothermometry over the last four glacial/interglacial cycles. *Marine Geology* **230** (1-2), 73–86.

Putnam, A.E., Denton, G.H., Schaefer, J.M., Barrell, D.J.A., Andersen, B.G., Finkel, R.C., Schwartz, R., Doughty, A.M., Kaplan, M.R. & Schluchter, C. (2010a). Glacier advance in southern middle-latitudes during the Antarctic Cold Reversal. *Nature Geosci* **3** (10), 700–704.

Putnam, A.E., Schaefer, J.M., Barrell, D.J.A., Vandergoes, M., Denton, G.H., Kaplan, M.R.,

Finkel, R.C., Schwartz, R., Goehring, B.M. & Kelley, S.E. (2010b). In situ cosmogenic 10Be production-rate calibration from the Southern Alps, New Zealand. *Quaternary Geochronology* **5** (4), 392–409.

Putnam, A.E., Schaefer, J.M., Denton, G.H., Barrell, D.J.A., Andersen, B.G., Koffman, T.N.B., Rowan, A. V, Finkel, R.C., Rood, D.H., Schwartz, R., Vandergoes, M.J., Plummer, M.A., Brocklehurst, S.H., Kelley, S.E. & Ladig, K.L. (2013a). Warming and glacier recession in the Rakaia valley, Southern Alps of New Zealand, during Heinrich Stadial 1. *Earth and Planetary Science Letters* **382**, 98–110.

Putnam, A.E., Schaefer, J.M., Denton, G.H., Barrell, D.J.A., Birkel, S.D., Andersen, B.G., Kaplan, M.R., Finkel, R.C., Schwartz, R. & Doughty, A.M. (2013b). The Last Glacial Maximum at 44°S documented by a 10Be moraine chronology at Lake Ohau, Southern Alps of New Zealand. *Quaternary Science Reviews* **62**, 114–141.

Putnam, A.E., Schaefer, J.M., Denton, G.H., Barrell, D.J.A., Finkel, R.C., Andersen, B.G., Schwartz, R., Chinn, T.J.H. & Doughty, A.M. (2012). Regional climate control of glaciers in New Zealand and Europe during the pre-industrial Holocene. *Nature Geosci* **5** (9), 627–630.

Rasmussen, S.O., Andersen, K.K., Svensson, A.M., Steffensen, J.P., Vinther, B.M., Clausen, H.B., Siggaard-Andersen, M.L., Johnsen, S.J., Larsen, L.B., Dahl-Jensen, D., Bigler, M., Röthlisberger, R., Fischer, H., Goto-Azuma, K., Hansson, M.E. & Ruth, U. (2006). A new Greenland ice core chronology for the last glacial termination. *J. Geophys. Res.* **111** (D6), D06102.

Rother, H., Fink, D., Shulmeister, J., Mifsud, C., Evans, M. & Pugh, J. (2014). The early rise and late demise of New Zealand's last glacial maximum. *Proceedings of the National Academy of Sciences* **111** (32), 11630–11635.

Rother, H., Shulmeister, J., Fink, D., Alexander, D. & Bell, D. (2015). Surface exposure chronology of the Waimakariri glacial sequence in the Southern Alps of New Zealand: Implications for MIS-2 ice extent and LGM glacial mass balance. *Earth and Planetary Science Letters* **429**, 69–81.

Ryan, M.T., Dunbar, G.B., Vandergoes, M.J., Neil, H.L., Hannah, M.J., Newnham, R.M., Bostock, H. & Alloway, B.V. (2012). Vegetation and climate in Southern Hemisphere mid-latitudes since 210 ka: new insights from marine and terrestrial pollen records from New Zealand. *Quaternary Science Reviews* **48**, 80–98.

Sagredo, E.A., Moreno, P.I., Villa-Martinez, R., Kaplan, M.R., Kubik, P.W. & Stern, C.R. (2011). Fluctuations of the Última Esperanza ice lobe (52°S), Chilean Patagonia, during the last glacial maximum and termination 1. *Geomorphology* **125** (1), 92–108.

Schaefer, J.M., Denton, G.H., Barrell, D.J.A., Ivy-Ochs, S., Kubik, P.W., Andersen, B.G., Phillips, F.M., Lowell, T. V & Schlüchter, C. (2006). Near-Synchronous Interhemispheric Termination of the Last Glacial Maximum in Mid-Latitudes. *Science* **312** (5779), 1510–1513.

Schaefer, J.M., Putnam, A.E., Denton, G.H., Kaplan, M.R., Birkel, S., Doughty, A.M., Kelley, S., Barrell, D.J.A.A., Finkel, R.C., Winckler, G., Anderson, R.F., Ninneman, U.S., Barker, S., Schwartz, R., Andersen, B.G. & Schluechter, C. (2015). The Southern Glacial Maximum 65,000 years ago and its Unfinished Termination. *Quaternary Science Reviews* **114**, 52–60.

Seidov, D. & Maslin, M. (2001). Atlantic ocean heat piracy and the bipolar climate see-saw during Heinrich and Dansgaard–Oeschger events. *Journal of Quaternary Science* **16** (4), 321–328.

Shulmeister, J., Fink, D. & Augustinus, P.C. (2005). A cosmogenic nuclide chronology of the

last glacial transition in North-West Nelson, New Zealand—new insights in Southern Hemisphere climate forcing during the last deglaciation. *Earth and Planetary Science Letters* **233** (3–4), 455–466.

Shulmeister, J., Fink, D., Hyatt, O.M., Thackray, G.D. & Rother, H. (2010). Cosmogenic 10Be and 26Al exposure ages of moraines in the Rakaia Valley, New Zealand and the nature of the last termination in New Zealand glacial systems. *Earth and Planetary Science Letters* **297** (3–4), 558–566.

Shulmeister, J., Goodwin, I., Renwick, J., Harle, K., Armand, L., McGlone, M.S.M., Cook, E., Dodson, J., Hesse, P.P., Mayewski, P. & Curran, M. (2004). The Southern Hemisphere westerlies in the Australasian sector over the last glacial cycle: a synthesis. *Quaternary International* **118-119**, 23–53.

Sikes, E.L., Howard, W.R., Samson, C.R., Mahan, T.S., Robertson, L.G. & Volkman, J.K. (2009). Southern Ocean seasonal temperature and Subtropical Front movement on the South Tasman Rise in the late Quaternary. *Paleoceanography* **24** (2), n/a–n/a.

Sime, L.C., Kohfeld, K.E., Le Quéré, C., Wolff, E.W., de Boer, A.M., Graham, R.M. & Bopp, L. (2013). Southern Hemisphere westerly wind changes during the Last Glacial Maximum: model-data comparison. *Quaternary Science Reviews* **64** (0), 104–120.

Stokes, C.R., Tarasov, L. & Dyke, A.S. (2012). Dynamics of the North American Ice Sheet Complex during its inception and build-up to the Last Glacial Maximum. *Quaternary Science Reviews* **50**, 86–104.

Stone, J.O. (2000). Air pressure and cosmogenic isotope production. *J. Geophys. Res.* **105** (B10), 23753–23759.

Sugden, D.E., Bentley, M.J., Fogwill, C.J., Hulton, N.R.J., McCulloch, R.D. & Purves, R.S. (2005). Late-glacial glacier events in southernmost South America: A blend of 'northern'and 'southern' hemispheric climatic signals? *Geografiska Annaler Series a-Physical Geography* **87A** (2), 273–288.

Sugden, D.E., McCulloch, R.D., Bory, A.J.M. & Hein, A.S. (2009). Influence of Patagonian glaciers on Antarctic dust deposition during the last glacial period. *Nature Geoscience* **2** (4), 281–285.

Sutherland, R., Kim, K., Zondervan, A. & McSaveney, M. (2007). Orbital forcing of mid-latitude Southern Hemisphere glaciation since 100 ka inferred from cosmogenic nuclide ages of moraine boulders from the Cascade Plateau, southwest New Zealand. *Geological Society of America Bulletin* **119** (3-4), 443–451.

Vandergoes, M.J., Newnham, R.M., Denton, G.H., Blaauw, M. & Barrell, D.J.A. (2013). The anatomy of Last Glacial Maximum climate variations in south Westland, New Zealand, derived from pollen records. *Quaternary Science Reviews* **74**, 215–229.

Vandergoes, M.J., Newnham, R.M., Preusser, F., Hendy, C.H., Lowell, T. V, Fitzsimons, S.J., Hogg, A.G., Kasper, H.U. & Schluchter, C. (2005). Regional insolation forcing of late Quaternary climate change in the Southern Hemisphere. *Nature* **436** (7048), 242–245.

Veres, D., Bazin, L., Landais, A., Toyé Mahamadou Kele, H., Lemieux-Dudon, B., Parrenin, F., Martinerie, P., Blayo, E., Blunier, T., Capron, E., Chappellaz, J., Rasmussen, S.O., Severi, M., Svensson, A., Vinther, B. & Wolff, E.W. (2013). The Antarctic ice core chronology (AICC2012): an optimized multi-parameter and multi-site dating approach for the last 120 thousand years. *Climate of the Past* **9** (4), 1733–1748.

Williams, P.W. (1996). A 230 ka record of glacial and interglacial events from Aurora Cave, Fiordland, New Zealand. *New Zealand Journal of Geology and Geophysics* **39** (2),

225–241.

Williams, P.W., McGlone, M., Neil, H. & Zhao, J.-X. (2015). A review of New Zealand palaeoclimate from the Last Interglacial to the global Last Glacial Maximum. *Quaternary Science Reviews* **110**, 92–106.

Wolff, E.W., Barbante, C., Becagli, S., Bigler, M., Boutron, C.F., Castellano, E., de Angelis, M., Federer, U., Fischer, H., Fundel, F., Hansson, M., Hutterli, M., Jonsell, U., Karlin, T., Kaufmann, P., Lambert, F., Littot, G.C., Mulvaney, R., Röthlisberger, R., Ruth, U., Severi, M., Siggaard-Andersen, M.L., Sime, L.C., Steffensen, J.P., Stocker, T.F., Traversi, R., Twarloh, B., Udisti, R., Wagenbach, D. & Wegner, A. (2010a). Changes in environment over the last 800,000 years from chemical analysis of the EPICA Dome C ice core. *Quaternary Science Reviews* **29** (1–2), 285–295.

Wolff, E.W., Chappellaz, J., Blunier, T., Rasmussen, S.O. & Svensson, A. (2010b). Millennial-scale variability during the last glacial: The ice core record. *Quaternary Science Reviews* **29** (21-22), 2828–2838.

Wolff, E.W., Fischer, H., Fundel, F., Ruth, U., Twarloh, B., Littot, G.C., Mulvaney, R., Röthlisberger, R., de Angelis, M., Boutron, C.F., Hansson, M., Jonsell, U., Hutterli, M.A., Lambert, F., Kaufmann, P., Stauffer, B., Stocker, T.F., Steffensen, J.P., Bigler, M., Siggaard-Andersen, M.L., Udisti, R., Becagli, S., Castellano, E., Severi, M., Wagenbach, D., Barbante, C., Gabrielli, P. & Gaspari, V. (2006). Southern Ocean sea-ice extent, productivity and iron flux over the past eight glacial cycles. *Nature* **440** (7083), 491–496.

Wolff, E.W., Fischer, H. & Rothlisberger, R. (2009). Glacial terminations as southern warmings without northern control. *Nature Geosci* **2** (3), 206–209.

9 Tables

Table 1. Details of the published literature compiled in this study, ordered by location and showing the latitude, longitude and total number of exposure ages compiled from the period 110-10 ka without and with (in brackets) author-identified outliers removed.

Glacier system	Lat. (°S)	Long. (°W/E)	Total no. ages		References
Patagonia					
Lago Bueno Aires	-46/-47	-71/-73	76	(64)	(Kaplan et al., 2004, 2005; Douglass et al., 2005, 2006; Glasser et al., 2012)
Río Bayo valley	-47	-73	3	(3)	(Glasser et al., 2006)
Nef valley	-47	-73	6	(5)	(Glasser et al., 2012)
Pueyrredón	-47/-48	-71/-73	19	(16)	(Hein et al., 2009, 2010, 2011; Glasser et al., 2012)
San Martín valley	-49	-72/-73	10	(10)	(Glasser et al., 2011)
Río Guanaco	-50	-73	21	(21)	(Murray et al., 2012)
Lago Argentino	-50	-73	30	(27)	(Ackert et al., 2008; Kaplan et al., 2011)
Torres del Paine	-51	-73/-74	54	(45)	(Fogwill, 2003; Fogwill & Kubik, 2005; Moreno et al., 2009; García et al., 2012)
Río Gallegos	-51/-52	-71/-72	7	(6)	(Kaplan et al., 2007; Evenson et al., 2009; Sagredo et al., 2011)
Magellan	-52/-53	-69/-71	17	(10)	(McCulloch et al., 2005; Kaplan et al., 2008, 2007)
BI-SSb	-53/-54	-68/-70	46	(34)	(McCulloch et al., 2005; Kaplan et al., 2007, 2008; Evenson et al., 2009; Darvill et al., 2015)
Total within Last Glacial Cycle			*289*	*(241)*	
New Zealand					
Cobb Valley	-41	173	12	(9)	(Shulmeister et al., 2005)
Taramakau	-43	171/172	34	(29)	(Barrows et al., 2013)
Arthur's Pass	-43	172	5	(4)	(Ivy-Ochs et al., 1999)
Waimakariri	-43	172	31	(29)	(Rother et al., 2015)
Rakaia Valley	-43/-44	171/172	55	(46)	(Shulmeister et al., 2010; Putnam et al., 2013a)
Cameron glacier	-43	171	10	(10)	(Putnam et al., 2012)
Franz Josef	-43/-44	170	6	(6)	(Barrows et al., 2007b)
Rangitata Valley	-43/-44	171	56	(51)	(Rother et al., 2014)
Pukaki	-44	170/171	169	(159)	(Schaefer et al., 2006; Putnam et al., 2010a; Kelley et al., 2014; Doughty et al., 2015; Schaefer et al., 2015)
Ohau	-44	170	91	(84)	(Kaplan et al., 2013; Putnam et al., 2013b)
Irishman Stream	-44	170	33	(31)	(Kaplan et al., 2010)
Cascade Plateau	-44	168	19	(14)	(Sutherland et al., 2007)
Boundary Stream Tarn	-44	170	10	(10)	(Putnam et al., 2010b)
Total within Last Glacial Cycle			*531*	*(482)*	

Table 2. The timing of culminations in glacial advances identified from relative cumulative probability density functions for New Zealand and Patagonia using the New Zealand production rate of Putnam et al. (2010), and using the Patagonian production rate (PPR) of Kaplan et al. (2011) for Patagonia. Values in italics indicate peaks that fail to resolve with only a small change in erosion rate. Values in bold are those quoted in our study and all other values show the effects of increasing the erosion rate or changing the production rate. Grey shading indicates the erosion rate required (to the nearest 1 mm ka^{-1}) to create a peak in New Zealand at the same time as Patagonia (e.g. a 6 mm ka^{-1} erosion rate is required to result in a peak in New Zealand at 13.9 ka, the same time as a peak in Patagonia with no erosion). The difference in timing between three closely-aligned peaks in Patagonia and New Zealand is given in the bottom row.

Timing of peaks											
Erosion rate	Patagonia (ka)										
0 mm ka^{-1}	**11.3**	**13.9**	*16.7*	**18.8**	**26.9**	**-**	**37.8**	**-**	**56.4**	-	-
0 mm ka^{-1} (PPR)	11.2	13.7	-	18.5	26.1	-	37.2	-	55.7	-	*93.3*
1 mm ka^{-1}	11.4	14.1	*16.9*	19.1	27.5	-	38.9	-	59.1	-	-
2 mm ka^{-1}	11.5	14.2	*17.1*	19.4	28.1	-	40.2	-	62.2	-	-
3 mm ka^{-1}	11.6	14.4	*17.3*	19.7	28.8	-	41.6	-	65.8	-	-
4 mm ka^{-1}	11.7	14.6	*17.6*	20.1	29.5	-	43.1	-	70.0	-	-
5 mm ka^{-1}	11.8	14.7	-	20.3	30.3	-	44.8	-	75.0	-	-
6 mm ka^{-1}	11.9	14.9	-	20.7	31.1	-	46.6	-	81.1	-	-
7 mm ka^{-1}	12.1	15.1	-	21.0	32.0	-	48.7	-	88.9	-	-
8 mm ka^{-1}	12.2	15.3	-	21.4	32.9	-	51.0	-	99.1	-	-
9 mm ka^{-1}	12.3	15.5	-	21.8	33.9	-	53.6	-	-	-	-
10 mm ka^{-1}	12.4	15.7	-	22.3	35.0	-	56.6	-	-	-	-
Erosion rate	New Zealand (ka)										
0 mm ka^{-1}	**-**	**13.0**	**-**	**18.1**	**26.6**	**32.7**	**-**	**41.3**	**-**	**65.3**	*89.7*
1 mm ka^{-1}	-	13.1	-	18.4	27.2	33.6	-	42.8	-	69.0	*96.9*
2 mm ka^{-1}	-	13.2	-	18.7	27.8	34.6	-	44.4	-	73.4	*105.7*
3 mm ka^{-1}	-	13.4	-	18.9	28.4	35.6	-	46.2	-	78.7	-
4 mm ka^{-1}	-	13.5	-	19.2	29.0	36.7	-	48.2	-	85.1	-
5 mm ka^{-1}	-	13.7		19.6	29.7	37.9	-	50.5	-	93.2	-
6 mm ka^{-1}	-	13.9	-	19.9	30.5	39.3	-	53.3	-	103.6	-
7 mm ka^{-1}	-	14.0	-	20.2	-	40.7	-	56.5	-	-	-
8 mm ka^{-1}	-	14.2	-	20.6	-	42.4	-	60.1	-	-	-
9 mm ka^{-1}	-	14.4	-	21.0	-	44.2	-	64.3	-	-	-
10 mm ka^{-1}	-	14.6	-	21.4	-	46.2	-	69.3	-	-	-
Difference (ka)		**0.9**	**0.7**	**0.3**							

10 Figure captions

Figure 1. Map of the Southern Hemisphere showing the modern positions of the Sub-Tropical Front (red), Sub-Antarctic Front (green) and Polar Front (blue) based on Orsi et al. (1995) and Carter et al. (2008), as well as the schematic core region of the Southern Westerly Winds (yellow-brown; Sime et al., 2013) and the locations of ice and marine core records referred to in the text. Note the latitudinal difference of the oceanic frontal systems around Patagonia compared to New Zealand.

Figure 2. (Left) Map of Patagonia, showing the hypothesised extent of the gLGM ice sheet from Coronato & Rabassa (2011) and -125 m bathymetric contour to give an impression of the likely drop in sea-level at the time. Glacial valleys or systems used in this study are labelled (A-K; corresponding to names on the right) as well as major oceanic circulations (blue arrows; Brown et al., 2001), Southern Westerly Wind direction (brown dashed arrows; Sime et al., 2013), and the Sub-Antarctic Front (green line; Orsi et al., 1995). (Right) Probability density functions for each glacial system consisting of all exposure ages (lighter shading) and with author-identified outliers removed (darker shading), normalised in both cases. The numbers of exposure ages relating to each system are shown without and with (in brackets) outliers removed.

Figure 3. (Left) Map of South Island, New Zealand, showing the hypothesised extent of the gLGM icefield from Barrell (2011) and -125 m bathymetric contour to give an impression of the likely drop in sea-level at the time. Glacial valleys or systems used in this study are labelled (A-K; corresponding to names on the right) as well as major oceanic circulations (blue arrows; Brown et al., 2001), Southern Westerly Wind direction (brown dashed arrows; Sime et al., 2013), and the Sub-Tropical Front (red line; Orsi et al., 1995). (Right) Probability density functions for each glacial system consisting of all exposure ages (lighter shading) and with author-identified outliers removed (darker shading), normalised in both cases. The numbers of exposure ages relating to each system are shown without and with (in brackets) outliers removed.

Figure 4. The compilation of ^{10}Be exposure ages from Patagonia and New Zealand used in this study (see Table 1), shown against the Marine Isotope Stages from Lisiecki & Raymo (2005) and the gLGM from Clark et al. (2009). (A and C) For Patagonia and New Zealand, respectively: all ^{10}Be exposure ages within 110-10 ka, including author-identified outliers, as mean ages with standard errors recalculated using the Putnam et al. (2010b) production rate, with no erosion rate applied. The exposure ages are colour-coded according to the glacial system from which they are derived, and associated references can be found in Table 1. (B and D) For Patagonia and New Zealand, respectively: normalised cumulative relative probability density function curves, calculated from all of the exposure ages shown in (A and C).

Figure 5. Examining the effects of calculation parameters on the overall spread of ages in our compilation. (A, B and C) Normalised probability density functions from Figure 4 without and with author-identified outliers removed. There is little resulting difference in the timing of peaks. (B) The effect of calculating all exposure ages from Patagonia with the Patagonian production rate of Kaplan et al. (2011). (D and E) The effect on the resulting normalised probability density functions of incrementally increasing the erosion rate by 1 mm ka^{-1} during the calculation of all ages in Patagonia and New Zealand. The timing of peaks can be found in Table 2. (F and G) The effect of altering the scaling scheme used. The scaling schemes are: the time-independent Lal (1991) and Stone (2000; St); Desilets et al. (2006; De); Dunai (2001; Du); Lifton et al. (2005; Li); and time-dependent Lal (1991) and Stone (2000; Lm). In (D, E, F and G), all author-identified outliers have been removed, the New Zealand production rate is used and, where relevant, no erosion rate is applied.

Figure 6. (A and B) Binned results from an analysis of skewness of probability density functions from individual moraine age populations in Patagonia and New Zealand as a crude proxy for differential inheritance signatures. The data suggest that inheritance cannot fully explain the consistent offset between Patagonia and New Zealand. (C and D) Skewness results against the number of exposure ages per moraine and age, respectively, demonstrating that these variables do not influence skewness (i.e. inheritance) in Patagonia more or less than New Zealand. (D) Younger moraines in both regions show greater skewness, indicating greater inheritance. See main text for discussion.

Figure 7. Orbital insolation parameters relevant to this study, from Berger & Loutre (1991). (A) LR04 benthic foraminiferal $\delta^{18}O$ stack (Lisiecki & Raymo, 2005), which shows a combined signature of global temperature and ice volume, (B) CO_2 record from EPICA Dome C (Lüthi et al., 2008), and (C) Northern Hemisphere summer (June) insolation intensity at 60°N. These three proxies show that global temperatures and Northern Hemisphere ice sheets followed Northern Hemisphere insolation during the last glacial cycle. (C) also shows Southern Hemisphere winter duration, given that decreasing northern summer insolation co-varies with increasing southern winter length (Huybers & Denton, 2008). (D) Southern Hemisphere summer (December) insolation intensity and (E) Southern Hemisphere seasonality at 60°S, 50°S, 40°S and 30°S. Seasonality values are calculated for each latitude by subtracting the June (winter) insolation from the December (summer) insolation at a given time, such that decreasing seasonality indicates cooler summers and warmer winters. These values are then normalised against the mean seasonality at each latitude for 110-10 ka. (F, G, H and I) Illustrations of decreasing CO_2 levels (F); Northern Hemisphere summer insolation intensity minima (G); Southern Hemisphere summer insolation intensity minima (H); and the broad overlap between the insolation minima in the Northern and Southern Hemispheres (I). The insolation intensity thresholds for these illustrations are entirely arbitrary: below 500 W m^{-2} for the Northern Hemisphere and below 490 W m^{-2} for the Southern Hemisphere (60˚S, except for the prolonged decreases at 93-85 ka and 47-34 ka, where threshold is raised). (J and K) The timing of peaks in our compilation for Patagonia and New Zealand, respectively, from Table 2. (L) Our ^{10}Be compilation from Patagonia and New Zealand with outliers removed.

Figure 8. A comparison of the timing of glacial advance culminations in the southern mid-latitudes during 110-10 ka with a range of other palaeoclimatic proxies. (A) The LR04 benthic foraminiferal stack (Lisiecki & Raymo, 2005). (B) The East Dronning Maud Land (EDML) ice core $\delta^{18}O$ record (EPICA, 2006); (D) the EPICA Dome C (EDC) ice core δD record (EPICA, 2006); and (E) the Byrd ice core $\delta^{18}O$ record (Blunier & Brook, 2001) as proxies for Antarctic temperature changes from different parts of the ice sheet. The EDML and EDC records are shown on the AICC2012 common timescale (Veres et al., 2013), whereas the Byrd ice core is plotted on its own timescale. (E) Faunal-based Sea Surface Temperature (SST) record from core SO136-GC3 as a proxy for regional temperature changes west of New Zealand (Barrows et al., 2007a). (F and G) Alkenone-derived SST reconstructions for ODP-1233 off the western coast of northern Patagonia (Kaiser et al., 2005) and for MD07-3128 off the western coast of southern Patagonia (Caniupán et al., 2011), both plotted on the same scale. (H and I) Records of opal flux from cores TN057-13 and -14 in the South Atlantic, south of the Polar Front, as a proxy for wind-driven upwelling (Anderson et al., 2009). Note that the scales are different. (J) Diatom-based reconstruction of sea ice extent from south of the Sub-Antarctic Front (Crosta et al., 2004), measured as the number of months per year that sea ice covered site SO136-111. (K) Ca^{2+} flux as recorded in the EDC ice core as a proxy for dust deposition over Antarctica, sourced predominantly from Patagonia (Fischer et al., 2007). (L) A record of Ice-Rafted Debris (IRD) from core MD07-3128 (Caniupán et al., 2011). (M and N) Culminations in the timing of glacial advances from Table 2. (O) Overlap between Northern Hemisphere and Southern Hemisphere summer insolation intensity from Figure 7. (P and Q) Our ^{10}Be compilation from Patagonia and New Zealand with outliers removed.

11 Supplementary material

11.1 Supplementary figure

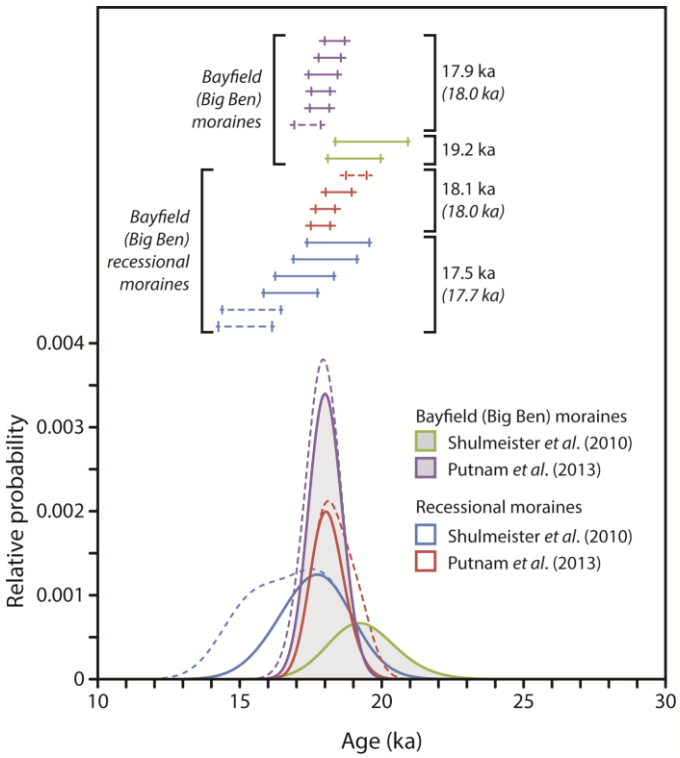

Supplementary figure. A comparison of the exposure ages produced by two different studies on the same moraines in the Rakaia Valley system (see Putnam et al. (2013a) for detailed discussion). Shulmeister et al. (2010) prepared samples at the University of Canterbury and conducted AMS isotopic analysis at the Australian Nuclear Science and Technology Organisation. Putnam et al. (2013a) prepared samples at the Lamont-Doherty Earth Observatory Cosmogenic Nuclide Laboratory and conducted AMS analysis at the Lawrence-Livermore National Laboratory Centre for Accelerator Mass Spectrometry. In all cases, dashed lines show where ages were rejected as outliers in the original studies. The upper horizontal lines are 2σ external uncertainties for ages calculated using the time-dependent scaling scheme (Lm) of Lal (1991) and Stone (2000), with vertical ticks showing 1σ internal uncertainties. The lower curves show Probability Density Functions (PDFs) for the moraine populations from each study, with and without outliers removed. The timing of peaks in these PDFs is shown next to the ages, with numbers in brackets indicating populations with outliers removed.

11.2 Supplementary data tables

Supplementary data tables can be found in the online version of this paper.